PHYSICAL REVIEW D **93,** 075029 (2016)

Dark matter direct detection with accelerometers

Peter W. Graham,[1] David E. Kaplan,[1,2,3,4] Jeremy Mardon,[1] Surjeet Rajendran,[3] and William A. Terrano[5,6]

[1]*Stanford Institute for Theoretical Physics, Department of Physics, Stanford University, Stanford, California 94305, USA*

[2]*Department of Physics & Astronomy, The Johns Hopkins University, Baltimore, Maryland 21218, USA*

[3]*Berkeley Center for Theoretical Physics, Department of Physics, University of California, Berkeley, California 94720, USA*

[4]*Kavli Institute for the Physics and Mathematics of the Universe (WPI), Todai Institutes for Advanced Study, University of Tokyo, Kashiwa 277-8583, Japan*

[5]*Center for Experimental Nuclear Physics and Astrophysics, University of Washington, Seattle, Washington 98195-4290, USA*

[6]*Physikdepartment, Technische Universität München, D-85748 Garching, Germany*

(Received 14 January 2016; published 20 April 2016)

The mass of the dark matter particle is unknown, and may be as low as $\sim 10^{-22}$ eV. The lighter part of this range, below ~eV, is relatively unexplored both theoretically and experimentally but contains an array of natural dark matter candidates. An example is the relaxion, a light boson predicted by cosmological solutions to the hierarchy problem. One of the few generic signals such light dark matter can produce is a time-oscillating, equivalence-principle-violating force. We propose searches for this using accelerometers, and consider in detail the examples of torsion balances, atom interferometry, and pulsar timing. These approaches have the potential to probe large parts of unexplored parameter space in the next several years. Thus such accelerometers provide radically new avenues for the direct detection of dark matter.

DOI: 10.1103/PhysRevD.93.075029

I. INTRODUCTION

The astrophysical and cosmological evidence for dark matter is overwhelming [1,2]. However, we know almost nothing about its fundamental properties. All we can say confidently about its mass is that it could range from astrophysically large scales to a lower limit where quantum pressure affects structure formation, currently estimated at $\sim 10^{-22}$ eV [3–10]. The type of particle and the nature of its interactions are unknown. Experimentally testing the vast range of well-motivated dark matter candidates is one of the most important objectives of modern physics.

For the purposes of direct detection, dark matter candidates can be roughly divided into two classes: particle-like or field-like. Because the local energy density of dark matter (DM) is $\rho_{\rm DM} \sim (0.04\ {\rm eV})^4$, if the dark matter mass (really momentum) is much greater than ~0.1 eV the phase-space density will be low and the dark matter acts more like a particle for the purposes of detection. If the mass (momentum) is much below this scale, then dark matter has a high phase-space density (many particles per de Broglie wavelength cubed) and is often well described as a classical field.[1] The weakly interacting massive particle (WIMP) [11] is the prototypical example of particle-like dark matter, while the axion [12–17] is the prototypical example of field-like dark matter. Traditional particle detection techniques are likely the optimal way to search for particle-like dark matter, at least in a very broad range of masses around the weak scale. There has been a significant, decades-long effort in direct detection of dark matter, focused on the WIMP. While the WIMP is well motivated, the lack of evidence for it to date at either direct detection experiments [18] or the LHC [19] suggests that the search for dark matter should be broadened to include other candidates. This paper will focus on novel ways to search for light, field-like dark matter. Such light dark matter has attracted a great deal of interest recently both theoretically and experimentally [20–56].

We wish to broaden the search for dark matter to the lighter part of the allowed range, but of course with an additional focus on the candidates that have the best motivation. Part of the motivation for both WIMPs and axions is that they can arise from solutions to tuning problems—the hierarchy problem and the strong *CP* problem respectively. In fact, the recently proposed cosmological solution to the hierarchy problem [57] predicts a light field, the relaxion—a light scalar which couples to matter through the Higgs portal. This is one of the types of particle that we focus on finding ways to search for in this paper. The other strong part of the motivation for WIMPs and axions is that they are good dark matter candidates, meaning that they have natural production mechanisms and are simple effective field theories which describe broad classes of higher-energy models. There are several types of light bosons which are also natural dark matter candidates. In particular, there are natural production mechanisms for

[1]In this case of course it must be a boson.

light bosons: misalignment production or decay of topological defects for scalars [15,16,58,59] and inflationary fluctuation production for vectors [43]. If a light boson does exist in the theory, these production mechanisms necessarily produce an abundance of this particle in the Universe, and it is natural for it to make up some or all of the dark matter.

Several direct detection searches for axion and hidden-photon dark matter are operating or are under construction [21,22,26,41,60,61]. In this paper we focus on two other well-motivated possibilities: scalars coupled to the Standard Model through the Higgs portal [46,62] and $B-L$ coupled vectors. As we show, such dark matter candidates can be powerfully probed with precision accelerometers—in particular through the time-oscillating, equivalence-principle violating-force that they exert on normal matter. Such accelerometers have been used to search for new forces or modifications of general relativity. Here we are considering the possibility that such a new force carrier is itself also the dark matter. Interestingly, the direct effect of the field as dark matter is expected to be significantly larger than its effect as a fifth-force mediator in future searches.

II. EXECUTIVE SUMMARY

(i) We investigate dark matter in the large mass range below ∼eV. Here dark matter behaves as an oscillating classical field. In terms of low-energy physics, there are only a handful of possible effective theories for dark matter in this part of parameter space, classified in Table I (see Sec. III). And in fact there are only four rough classes of detectable effects of such dark matter: spin effects, electromagnetic effects, accelerations, and variations of fundamental constants.

(ii) Direct detection experiments have already been designed to search for the spin and electromagnetic couplings (e.g. axion detectors). Here we focus on the equivalence-principle (EP)-violating acceleration caused by dark matter, which is not currently being searched for in any experiment. This effect is generic for both scalar and vector DM, two natural candidates being a scalar coupled through the Higgs portal and a vector coupled to $B-L$ charge. In addition we point out a new way of seeing the variation of fundamental constants using pulsar timing arrays.

(iii) This DM-induced acceleration oscillates in time with a fixed frequency and long coherence time ($\gtrsim 10^6$ periods) and points in a random direction (fixed in the Galactic frame over a coherence time). These features distinguish it from backgrounds such as seismic noise. The amplitude of the acceleration, combined with its distinctive features, make the DM signal significantly easier to search for over a wide DM mass range than static EP violation (caused by the same light field sourced by the Earth). See Sec. IV.

(iv) Existing accelerometer technology designed to search for static EP violation is automatically also sensitive to a DM-induced signal. In Sec. V A we examine the potential sensitivity of torsion pendulum setups, for example as used by the Eöt-Wash group [63]. These benefit significantly from the random direction of the DM signal, which avoids the $\sim 10^{-3}$ suppression suffered in searches for a vertical acceleration sourced by the Earth. The impressive sensitivity of these setups means that even a reanalysis of existing data will be able to probe new DM parameter space. With the technology upgrades expected over the next

TABLE I. The leading couplings of light bosonic dark matter (ϕ, a, A'_μ, and $h'_{\mu\nu}$) to Standard Model fields, and the oscillating physical effects they cause. h, $G^{\mu\nu}$, $F^{\mu\nu}$, ψ, and $T^{\mu\nu}$ represent respectively Standard Model Higgs, gluon, photon, and fermion fields, and the energy-momentum tensor, or operators of that form. The last column indicates DM searches currently existing or under construction. A star ($\star$) marks where the searches we propose would lie. We note that questions remain about validity, naturalness and allowed interactions in theories of massive spin-2 fields.

Spin	Type	Operator	Interaction	Oscillating DM Effects	Searches
0	Scalar	$\phi h^\dagger h$, $\phi \mathcal{O}_{\rm SM}$	Higgs portal/dilaton	m_e, m_p, α variation	Atomic clocks [64]
				Acceleration	$\star$
	Pseudo-scalar	$aG^{\mu\nu}\tilde{G}_{\mu\nu}$	Axion-QCD	Nucleon EDM	CASPEr [26]
		$aF^{\mu\nu}\tilde{F}_{\mu\nu}$	Axion-E&M	EMF along B field	ADMX [21]
		$(\partial_\mu a)\bar{\psi}\gamma^\mu\gamma_5\psi$	Axion-fermion	Spin torque	CASPEr [26]
1	Vector	$A'_\mu\bar{\psi}\gamma^\mu\psi$	Minimally coupled	Acceleration	$\star$
		$F'_{\mu\nu}F^{\mu\nu}$	Vector–photon mixing	EMF in vacuum	DM Radio [41], ADMX
		$F'_{\mu\nu}\bar{\psi}\sigma^{\mu\nu}\psi$	Dipole operator	Spin torque	CASPEr [26]
	Axial-vector	$A'_\mu\bar{\psi}\gamma^\mu\gamma^5\psi$	Minimally coupled	Spin torque	CASPEr [26]
2 (?)	Tensor	$h'_{\mu\nu}T^{\mu\nu}$(?)	Gravity-like	Gravitational wave-like	Gravitational wave detectors?

several years, they will reach into unconstrained parameter space by many orders of magnitude in mass and coupling strength.

(v) Atom interferometers are another type of high-precision accelerometer which can be sensitive to light field DM. As we discuss in Sec. V B, these are also expected to reach deep into currently unconstrained parameter space over the next several years.

(vi) Two other potentially powerful experimental options are lunar laser ranging and pulsar timing arrays; see Secs. V C and V D. In both cases, a reanalysis of existing data should be able to constrain new DM parameter space or even uncover a signal, and expected upgrades over the next few years should improve their reach further. Pulsar timing arrays in particular can be the most powerful probe of scalar DM at the lowest frequencies.

(vii) Our main results are shown in Figs. 2, 3 and 4, respectively for a $B-L$ coupled vector, a scalar coupled through the Higgs portal, and a scalar coupled to the electron mass operator. For the latter scalar coupling, a non-fine-tuned part of parameter space appears reachable in the near to mid term, while for the former scalar coupling this looks extremely difficult. However in both cases there is a large reach into fine-tuned but otherwise unconstrained parameter space. The projected reach for the $B-L$ coupled vector is particularly striking, extending many orders of magnitude into unprobed parameter space.

III. THEORETICAL LANDSCAPE OF LIGHT DARK MATTER

In this section, for theoretically minded readers, we categorize the range of possible light field dark matter candidates and their leading physical effects.

Light bosons are a well-motivated and underexplored class of dark matter candidates. While the allowed mass range is vast, the types of fields and natural couplings are limited. The leading interactions are shown in Table I. We focus on these operators since operators of higher dimension with linear couplings will have a lesser impact and will generate these lower-dimension operators via loops. In addition, we ignore operators with quadratic couplings (such as $\phi^2 h^\dagger h$), as their impact will be significantly smaller. We postpone discussion of spin-2 candidates for future work, since there are questions about the range of validity, degree of fine-tuning, and allowed interactions of massive spin-2 fields (see e.g. Refs. [65–67]). Finally, we do not consider massive bosons of spin 3 or higher, since we know of no effective field theory valid parametrically above their mass.

Interestingly there are not too many possibilities for light bosonic field dark matter, and it appears possible to design direct detection experiments to probe them all. The state of light bosonic dark matter in the Galaxy is well described as a random classical field that

(i) oscillates at an angular frequency equal to the dark matter mass, m,

(ii) is locally coherent over $\sim 10^6$ oscillations (meaning a 1 part in 10^6 frequency spread), and

(iii) has a local energy density of $\rho \sim (.04\ \mathrm{eV})^4 \sim m^2\phi^2$, where ϕ is the boson.

The first is simply true of a nonrelativistic field. The second is due to the fact that the virial velocity of local dark matter is $v \simeq 10^{-3}$ and the field should be coherent over a de Broglie wavelength $1/(mv)$, and thus for a time $\sim 1/(mv^2) \simeq 10^6/m$. The third assumes any of the standard halo profiles for dark matter, and thus makes a prediction for the amplitude of the field.[2] We note in addition that the gradient of a bosonic DM field is associated with its local velocity, which we assume to be random in the Galactic rest frame.

As a result of these oscillations, the dark matter acts as a time-dependent source term for the Standard Model operators given in Table I. This leads to time-dependent signals with the same frequency and phase as the dark matter field. The experimental signals can be roughly divided into three categories. First, the *axion-gluon, axion-fermion, vector dipole and axial-vector* couplings produce spin-dependent forces or signals. Proposals have been made to detect such dark matter, notably though detection of an oscillating neutron electric dipole moment and/or an "axion wind" (which exerts a torque on particles' spins) [25,26], which should in principle also be sensitive to vectors coupled through the dipole operator, and axial vectors. Independently of their cosmic abundance, these fields can also be searched for in experiments attempting to source and detect a spin-dependent force [70–73], although the DM searches have sensitivity to significantly smaller couplings.

The second category of experimental signals comes from the *vector-photon mixing and axion-photon coupling*, both of which can produce an effective electromotive force which can drive electric currents. The axion-photon coupling results in an EMF in the presence of a background magnetic field, and is being searched for in this way by ADMX [21]. Vector DM with vector-photon mixing generates an EMF in vacuum inside a shield, which will be searched for, for example, by the recently proposed DM Radio [41]. Again, these fields can also be searched for independently of their cosmic abundance, but with less

[2]Of course, ultralight bosons may also make up a subcomponent of DM with a significantly lower density. This makes it interesting to consider masses below the bound of $m_{\mathrm{DM}} \gtrsim 10^{-22}$ eV, which only applied to the dominant DM component. In addition, recent simulations of $\sim 10^{-22}$ eV mass DM [68,69] find $\mathcal{O}(1)$ density fluctuations over scales of order the de Broglie wavelength, implying an extra $\mathcal{O}(1)$ uncertainty in the local DM density beyond that for WIMP DM.

reach in coupling—in this case with experiments that search for transmission of electromagnetic radiation through a shield [31,39,74].

The third category comes from the *Higgs portal, minimal vector, and gravity-like* couplings, all of which can produce a coherent time-dependent EP-violating force on macroscopic matter, as well as an oscillation of Standard Model parameters. Exploiting these effects is the central point of this article.

Scalar couplings In the case of the scalar, there are a number of potentially important couplings to Standard Model fields. For example, a linear coupling to quark mass or electron mass operators will produce the time-dependent, EP-violating forces we are interested in. We focus in this paper on the linear coupling to the Higgs for several reasons.

(i) Universality: The coupling to the Higgs produces (different) couplings to the electron, proton, and neutron masses and thus, in terms of a single parameter, reproduces all of the interesting effects.

(ii) IR dominance: The scalar coupling to the Higgs is the lowest-dimension coupling allowed, and therefore any other linear coupling to Standard Model operators will generate this coupling at loop level, whereas the opposite cannot be said (as there are no divergent graphs for higher-dimensional operators). In addition, it is plausible that the UV theory produces this operator with a larger effective coefficient in the IR than all others due to its low dimension.

(iii) Naturalness: For a given ϕ mass, m, and coupling, $b\phi h^\dagger h$, naturalness only requires the coupling to be smaller than the mass, i.e. $b \lesssim m$ (having b larger than $\sim$ the Lagrangian mass parameter m_0 would destabilize the ϕ potential, but tuning b to be very close to this critical point allows the physical ϕ mass to be much smaller than b). Higgs loops also produce a tadpole term for ϕ with coefficient of order $b\Lambda^2$, where Λ is the scale at which Higgs loops are cut off. In the natural regime, $m_\phi \gtrsim b$, the linear term will produce a vacuum expectation value for ϕ of size $\sim b\Lambda^2/m^2$, and thus a contribution to the Higgs mass squared smaller than Λ^2, i.e. smaller than the direct quantum corrections to the Higgs mass. Thus, this coupling does not contribute to the naturalness story of the Higgs, and naturalness constraints on b do not depend upon the UV cutoff of the Standard Model. This is different from all other Standard Model operators ϕ could couple to, where the naturalness of its own mass would also depend on the cutoff scale of Standard Model loops.

In addition this direct coupling to the Higgs is interesting because it is the defining coupling of the scalar "relaxion" in dynamical relaxation solutions of the hierarchy problem [57]. While the last constraint makes the Higgs coupling especially interesting, there are individual couplings (e.g., to quark and electron masses) which can be both natural and more experimentally accessible (for a sufficiently low cutoff). We include a direct coupling to the electron mass in our projections as one interesting example.

Vector couplings A minimally coupled vector, which is anomaly free (with respect to mixed anomalies with the Standard Model gauge groups), and allows all Standard Model Yukawa couplings, is any linear combination of hypercharge and baryon minus lepton number ($B-L$). However, there are more generally a number of allowed vector couplings to the Standard Model.

(i) Flavor-blind, anomaly-free: $(B-L)+Y \to (B-L)+QED$. The latter part acts as a dark photon and will be picked up by those searches. However, bounds on the dark photon are tremendously weaker than bounds on $B-L$, since a dark photon puts a negligible force on neutral matter.

(ii) Flavor-blind, anomalous: B and L are anomalous symmetries, and a field coupled to them would produce a force on matter. Because of the anomaly, the longitudinal mode of such a vector would become strongly coupled at $\sim 4\pi m/g$, where m and g are the mass and coupling (assuming charges of order unity). This is the highest scale where new fermions could appear to cancel the anomaly (with Yukawa couplings of 4π), and thus we would require $\sim 4\pi m/g \gtrsim 1$ TeV, which we will see is difficult (but possible) to probe. Most combinations of B and L will have a similar degree of EP violation between different isotopes (except for B, which has larger suppression and is similar to the scalar).

(iii) Flavor-dependent, anomaly-free: It is easy to construct anomaly-free gauge symmetries with flavor-dependent charges. However, the required fermion masses in the Standard Model explicitly break such symmetries, which again implies a cutoff at some higher scale. For example, if electrons have an axial charge, and muons have the opposite axial charge, the explicit breaking of the gauge symmetry due to the muon Yukawa coupling, y_μ, will induce strong coupling for the longitudinal mode at a scale $\sim(4\pi/y_\mu)(m/g)$ (which is a weaker constraint than the anomalous case). By far the weakest strong coupling constraint is on a coupling to the difference of lepton flavors, such as $L_e - L_\mu$, which would only be violated by certain neutrino mixing terms. Vector bosons coupled to fermions of the first generation would produce similar effects to that of $B-L$, whereas couplings to second and third generations only will be much harder to test.

Thus, not only is a vector coupled to $B-L$ simplest from a theoretical point of view, but searching for its effects will also cover the effects of many other classes of vectors.

Thus, in this paper we will only consider vectors coupled to $B-L$ charge.

We note that vector DM must point in a particular direction, determined by both its production mechanism and the galactic formation/virialization processes. We assume this direction to be completely random, and to change over a coherence length/time.

IV. EP-VIOLATING SIGNATURES

A. Discussion

The DM described above causes an equivalence-principle-violating acceleration on test bodies, which oscillates in time at the natural frequency of the dark matter (equal to its mass). This is of great benefit to experiments searching for this signal, since it is a fundamental frequency of nature unrelated to anything generated by the laboratory or the experiment itself. Compare this with searches for static equivalence-principle-violating forces in which systematic effects such as gravitational gradients can mimic the signal. Handling these systematics is most difficult for static signals and is much less of a problem in searches for the very distinctive DM signal. In Sec. V A, we consider this explicitly in the concrete setup of torsion pendulums. In addition, the narrow frequency spread of the signal could also enable resonant schemes that lead to signal amplification.

The force on a test body from the dark matter points in a direction that is uncorrelated with anything in the laboratory and is fixed in the frame of the Galaxy over the coherence time. This is particularly beneficial in torsion pendulum experiments (discussed in more detail below), which suffer a $\sim 10^{-3}$ suppression in searches for a vertical force sourced by the Earth, but suffer no such suppression in a DM search. In the case of the $B-L$ coupled vector, for example, the force points in the direction of the vector's electric field, which is unknown. In the case of the scalar, the force points in the direction of the local gradient in the scalar field (its momentum). In either case the direction and magnitude of the force change by $\mathcal{O}(1)$ amounts on time scales of $10^6/m$, the coherence time of the dark matter. Of course, since the force is set in the Galactic frame, in the Earth frame it will also have a daily (and yearly) modulation. This modulation is useful because it allows us to distinguish the dark matter force from many backgrounds which arise from objects fixed on the Earth, for example static gravity gradients.

Given these advantages, what is the optimal way to measure these dark-matter-induced accelerations? Current accelerometer technologies are fundamentally sensors of position. The position of a test body subject to an acceleration a at a frequency m will oscillate with an amplitude $\Delta x \sim (a/m^2)$. These modulations of position can be measured with high-precision interferometers (either optical or atomic). Since displacement (as opposed to acceleration) is a relative quantity, this scheme can only measure relative accelerations, for example between two test bodies. The dark matter can induce such a relative acceleration in two ways. First, if the test bodies are physically separated by some distance, the value of the dark matter field at the two locations will be different, resulting in different forces being exerted on the two objects. This can produce a signal in gravitational-wave detectors, but with a significant suppression at lower frequencies due to the reliance on the small dark matter gradient ($\sim mv$), as was discussed in Ref. [46].

Second, if the composition of the two bodies is different, they will experience different accelerations, since the force exerted by the dark matter violates the equivalence principle. The size of this effect is suppressed by the degree of EP violation between the test-body materials. However, since the effect is independent of the physical separation of the test bodies, it does not suffer the extra gradient suppression seen in the effect relying on physical separation. It also allows experiments to be designed to be insensitive to the time-varying Newtonian gravitational backgrounds, which are known to be significant below ~ 10 Hz [75]. This is extremely beneficial since the measurable displacement of the text bodies increases as $1/m^2$, making accelerometers generally most sensitive at low frequencies.

The scalar DM considered in this paper can also produce oscillations of fundamental "constants," such as the electron mass or fine-structure constant. This approach was considered in Refs. [46,64] (using comparisons of different atomic clocks) and in Ref. [47] (using resonant mass detectors), and is considered again here in Sec. V D (using pulsar timing arrays). The proposed atomic clock searches would be sensitive at the lowest possible DM masses, and therefore overlap somewhat with the searches we consider here. We find the searches we propose to be generally more powerful, although the projections rely on assumptions about the development of different technologies, and have different relative strengths for different types of coupling.

We now focus on the Higgs-coupled scalar and the $B-L$ coupled vector as two naturally light DM candidates. We also consider a scalar coupled to the electron mass operator, as an example of the range of possible nonrenormalizable scalar couplings. These all induce a time-oscillating, EP-violating force on accelerometers (bulk matter or atoms). Searches for this effect constitute DM direct detection experiments, with the signal resulting from the direct contact interaction between the DM and normal matter, similar to axion or gravitational-wave detection.

B. $B-L$ vector DM

We begin with $B-L$ coupled vector dark matter. Such a light vector field behaves very similarly to a coherent electromagnetic field, except for its mass term and the fact that it also couples to neutrons. Its coupling can produce

new forces in two distinct and important ways. First, it produces a static force between clumps of matter (such as between the Earth and a test mass), and this force is constrained both by tests of the inverse square law and of the EP, depending on the vector mass (see, for example, Ref. [76]). Second, as we present in this paper, if the vector makes up a portion of the dark matter, it directly induces an oscillating (time-dependent) EP-violating force directly on matter. As discussed above, this points in a random direction which is expected to change over every coherence time. For a $B-L$ coupling, the dominant EP-violating effect is due to the relative neutron fraction of different atoms. In searches for a static effect, the force arises due to vector exchange between source and test masses, and (for distances shorter than the Compton wavelength of the boson) is

$$F_{\text{EP-static}} \simeq g_{B-L}^2 \Delta_{B-L} \left(\frac{A_S - Z_S}{A_S}\right) \frac{M_S M_{A_i}}{m_N^2} \frac{1}{R^2}. \quad (1)$$

Here g_{B-L} is the coupling strength of the vector, A_S and Z_S are the atomic weight and number of the source, R is the separation between the source and test bodies, M_S and M_A are their masses, m_N is the nucleon mass, and Δ_{B-L} is the degree of EP violation of the two test bodies, given by

$$\Delta_{B-L} = \frac{Z_1}{A_1} - \frac{Z_2}{A_2}, \quad (2)$$

where $A_{1,2}$ and $Z_{1,2}$ are the atomic weight and number of the two test bodies. Assuming the vectors are the dominant component of dark matter, their density is $\rho_{\text{DM}} \simeq m_A^2 A^\mu_{B-L} A^{B-L}_\mu \simeq \partial_t A_i^{B-L} \partial_t A^i_{B-L}$ (where we neglect the small spatial gradients). From the equations of motion, matter couples to $\partial_t A_i^{B-L} \simeq E_i^{B-L}$ as in normal electromagnetism, but with the neutron having the same charge as the proton. Thus, the magnitude of the EP-violating force is simply

$$F_{\text{EP-DM}} = g_{B-L} E^{B-L} \Delta_{B-L} \frac{M_{A_i}}{m_N} \simeq g_{B-L} \sqrt{\rho_{\text{DM}}} \Delta_{B-L} \frac{M_{A_i}}{m_N} \quad (3)$$

leading to a relative acceleration of

$$\Delta a_{\text{DM}} \simeq g \left(\frac{g_{B-L}}{2 \times 10^{-11}}\right) \Delta_{B-L}, \quad (4)$$

where $g \simeq 9.8\ \text{ms}^{-2}$.

Comparing the dark-matter-induced signal to the static force signal generated by the Earth, we get the simple formula for the ratio of acceleration amplitudes:

$$\frac{a_{\text{DM}}}{a_{\text{static}}} \simeq \frac{1}{g_{B-L}} \frac{m_N \sqrt{\rho_{\text{DM}}}}{m_{\text{Pl}}^2 g} \left(\frac{A_S - Z_S}{A_S}\right) \sim \frac{\frac{1}{4} \times 10^{-27}}{g_{B-L}}. \quad (5)$$

The $\mathcal{O}(10^{-3})$ suppression of the static effect in the Eöt-Wash experiment means that the dark matter produces a larger acceleration for couplings smaller than 10^{-24}–10^{-25}. As we see in Fig. 2, current bounds already push the coupling below this limit, and thus if $B-L$ coupled vectors make up all the dark matter, their effect on the Eöt-Wash torsion pendulums is larger than the static contribution in the entire remaining low-mass parameter space.

C. Higgs-portal scalar DM

We now turn to the more complicated case of a scalar linearly coupled to the Higgs mass operator, $\mathcal{L} \supset b\phi|\mathcal{H}|^2$. This translates in a relatively straightforward way to a linear coupling of ϕ to all Standard Model fields. To compute the effects on matter, we need the couplings to quarks and leptons, and the estimates of the coupling to neutrons, protons and nuclei (as parametrized in Ref. [62]):

$$\mathcal{L} \supset \frac{b\phi}{m_h^2} \langle h \rangle g_{h\psi\psi} \overline{\psi}\psi \quad (6)$$

where $\langle h \rangle = 246$ GeV and $m_h = 125$ GeV are the Higgs expectation value and mass. The ψ are fermions, and for quarks and leptons, it is simple to compute the leading coupling; minimizing the Higgs potential and treating ϕ as a background field, one gets $g_{hqq} = m_q/\langle h \rangle$ and $g_{h\ell\ell} = m_\ell/\langle h \rangle$ respectively. The universal coupling to nucleons has significant uncertainty, and we take $g_{hNN} = 200\ \text{MeV}/\langle h \rangle \simeq 10^{-3}$ in quoting our bounds. One can see this as a reasonable estimate from two contributions. First, if one integrates out the three heavy quarks—top, bottom, and charm—their mass thresholds depend on the scalar, ϕ, and one can compute contributions to the one-loop strong coupling scale, treating ϕ as a background field:

$$\Lambda_{\text{QCD}} \to \Lambda_{\text{QCD}} \left(1 + \frac{2}{9} \frac{b\phi}{m_h^2}\right) \quad (7)$$

which should produce a coupling to nucleons with $g_{hNN} \simeq (2/9) m_N/\langle h \rangle$, taking the nucleon mass, m_N, to scale essentially linearly with Λ_{QCD}. The $(2/9) = (b_3^c - b_3)/b_3^c$, where b_3^c, b_3 are the beta-function coefficients of QCD just below the charm mass and just above the top mass respectively. The other significant contribution should come from the strange mass contribution to nucleon masses, according to chiral perturbation theory. The contribution to the coupling is of the form

$$\frac{b\phi}{m_h^2} m_N f_s^N \overline{N} N, \quad \text{with} \quad f_s^N \equiv \frac{m_s}{m_N} \frac{\partial m_N}{\partial m_s}. \quad (8)$$

Recent lattice calculations, done at the physical point in parameter space, obtained $f_s^N \simeq 0.113 \pm 0.053$ [77].[3] Finally, the scalar, ϕ will have a coupling to photons at one loop by integrating out charged fermions and W bosons. This contribution is suppressed by a power of the fine-structure constant, α, and adds only a tiny correction to the scalar coupling to matter.

The force on matter violates EP. One reason is that the scalar couplings to neutrons and protons are not precisely proportional to their masses, and differ roughly by the lightest quark masses over the QCD scale, or $\delta \sim$ few $\times 10^{-3}$ [62]. When testing relative forces between different materials, the differential acceleration due to this difference in relative coupling would be proportional to this δ as well as the factor $\Delta_{B-L} = (Z_1/A_1 - Z_2/A_2)$, where $Z_{1,2}$ and $A_{1,2}$ are the atomic number and mass respectively of the two materials. In typical experiments testing EP, Δ_{B-L} is typically a few percent (see for example Ref. [63]).

However, a larger effect should come from the nuclear binding energy differences, especially when comparing light and heavy elements. This is because the binding energy should scale differently with $\Lambda_{\rm QCD}$ and the light quark masses than the nucleon masses do, and thus elements with the largest differences in binding energy per nucleon should produce the largest effect.

Let us see this explicitly. The mass of an atom is

$$M_A = Nm_n + Zm_p + A\mathcal{E}_B + Zm_e \tag{9}$$

where N, Z, and A are the neutron number, atomic number, and atomic weight and m_n, m_p, and m_e are the neutron, proton, and electron masses respectively, and $\mathcal{E}_B$ is the binding energy per nucleon (and is negative). This can be parametrized roughly as

$$M_A = Am_p + N\delta m_N + A\mathcal{E}_B + Zm_e \tag{10}$$

$$\to Am_n\left(1 + c_N\frac{b\phi}{m_h^2}\right) - Z\delta m_N\left(1 + c_q\frac{b\phi}{m_h^2}\right) + A\mathcal{E}_B\left(1 + c_B\frac{b\phi}{m_h^2}\right) + Zm_e\left(1 + \frac{b\phi}{m_h^2}\right), \tag{11}$$

where the second line comes from turning on a background ϕ. Here $\delta m_N = m_n - m_p$, $c_N \approx 200$ MeV$/m_N$, $c_q \approx \mathcal{O}(1)$, and c_B is expected to be somewhere between c_N and $\mathcal{O}(1)$. The c_q coupling is mostly due to the scaling of the nucleon mass difference with the up and down quark mass difference (and a negligible effect from the electromagnetic contribution to the nucleon masses), while c_B is due to the scaling of the binding energy with respect to the QCD scale, strange quark mass, and light quark masses.

Since the coupling of ϕ to the atom represents a potential energy for the atom in the presence of the background field, a nonzero gradient for ϕ produces a force on atoms. As discussed above, the gradient of the ϕ DM field is associated with its local velocity. In the Earth's frame it averages to the direction of motion of the Earth through the DM halo, with a random component that changes over a coherence time. The acceleration of an element i due to a background ϕ is proportional to the linear coupling of ϕ to the atom, divided by the atom's mass, or

$$a_i \simeq \nabla\phi\left(c_N - \frac{Z_i}{A_i}\frac{(c_q - c_N)\delta m_N - (1 - c_N)m_e}{m_n} + (c_B - c_N)\frac{\mathcal{E}_{B_i}}{m_n}\right)\frac{b}{m_h^2}. \tag{12}$$

The second and third terms in parentheses give rise to different accelerations for different materials (i.e. EP violation). The effect is typically dominated by the difference in binding energies, so long as $c_B \neq c_N$. c_B and c_N have not been precisely measured, but a close cancellation is not expected. In particular, c_N is expected to receive a contribution from m_s at the $\mathcal{O}(0.1)$ level [Eq. (8)], whereas c_B is not. The binding energy is also expected to have a dependence on the pion mass, and consequently on the up and down quark masses, that will contribute to $c_B - c_N$ (although some recent lattice calculations have found this contribution to be small [79]). We therefore take $c_B - c_N = 0.1$ in our calculations, which we assume to be a reasonably conservative estimate.[4]

In an accelerometer, scalar dark matter will put a direct (time-dependent) EP-violating force on the test masses, which will point in a random direction. If the field makes up all the dark matter abundance, then locally $\rho_{\rm DM} \simeq m_\phi^2\phi^2 \approx 0.3$ GeV$/$cm$^3 \approx (0.04$ eV$)^4$. We can replace the gradient of ϕ with the momentum in the field, $\nabla\phi \to m_\phi v\phi$, where $v \approx 10^{-3}$ is the local dark matter velocity. This gives a relative acceleration between two test mass materials of

$$\Delta a_{\rm DM} = v\sqrt{\rho_{\rm DM}}\frac{b}{m_h^2}\Delta_{\phi|H|^2}, \tag{13}$$

where

$$\Delta_{\phi|H|^2} = \left[(c_B - c_N)\frac{\mathcal{E}_{B_1} - \mathcal{E}_{B_2}}{m_n} - \left(\frac{Z_1}{A_1} - \frac{Z_2}{A_2}\right) \times \frac{(c_q - c_N)\delta m_N - (1 - c_N)m_e}{m_n}\right]. \tag{14}$$

[3]However, competing calculations extrapolated to the physical point measure disparate values; see e.g. Ref. [78], and Fig. 2 of Ref. [77].

[4]Strictly speaking, c_B should depend on the species of atom, but at this point we cannot do better than an $\mathcal{O}(1)$ estimate.

We take $(c_q - c_N) \approx (1 - c_N) \approx 1$, and $(c_B - c_N) \approx 0.1$. For example, with Al/Be test masses, the difference in binding energies dominates ($\mathcal{E}_{B_1} - \mathcal{E}_{B_2} = 1.87$ MeV), and $\Delta_{\phi|H|^2} \approx 2 \times 10^{-4}$. On the other hand, for ^{85}Rb/^{87}Rb test masses, the second term is larger, and $\Delta_{\phi|H|^2} \approx 7 \times 10^{-6}$.

The comparison between the DM-induced signal and the static effect generated by the Earth is now

$$\frac{\Delta a_{\rm DM}}{\Delta a_{\rm static}} \simeq v\sqrt{\rho_{\rm DM}}\left(c_N \frac{b}{m_h^2} m_{\rm Pl}^2 g\right)^{-1} \sim \frac{10^{-16}\ \text{eV}}{b}. \quad (15)$$

Thus, the DM force is stronger when the coupling (and on the naturalness line, the mass) is smaller than 10^{-16} eV. Again, Eöt-Wash tests of static EP violation receive an extra relative suppression of $\sim 10^3$ on top of this estimate, because they are only sensitive to the horizontal force from the center of the Earth [63]. Using the numbers given above, the static bounds on a $B-L$ coupled vector of Ref. [63] can be converted into bounds on the scalar using $b \equiv 2.6 \times 10^{13} g_{B-L}\sqrt{\Delta_{B-L}/\Delta_{\phi|H|^2}}$, where $\Delta_{B-L} = 0.037$ and $\Delta_{\phi|H|^2} = 4 \times 10^{-4}$ give the degree of EP violation for the Al/Be test mass combination used to set the limits.

D. Scalar coupled to electron mass

As an example of an alternate coupling of scalar DM, we also consider a dilaton-like coupling only to the electron mass operator,

$$\mathcal{L} \supset y_{\phi ee}\phi\bar{e}e. \quad (16)$$

For naturalness the scalar's mass should satisfy (schematically) $m \gtrsim y_{\phi ee}\Lambda/4\pi$, where Λ is the scale at which electron loops are cut off, and we assume $\Lambda \gtrsim$ TeV.

The static EP violation sourced by the Earth is related to that in the $B-L$ case by

$$\begin{aligned}\Delta\vec{a}|_{\phi\bar{e}e,\rm static} &= y_{\phi ee}^2 N_{e,\rm source}\left(\frac{Z_1}{A_1 m_N} - \frac{Z_2}{A_2 m_N}\right)\frac{\hat{r}}{4\pi r^2} \\ &= \frac{y_{\phi ee}^2}{g_{B-L}^2}\frac{N_{e,\rm source}}{N_{n,\rm source}} \times \Delta\vec{a}|_{B-L,\rm static}. \end{aligned} \quad (17)$$

Since the Earth has $N_e \approx N_n$, we can therefore just use $y_{\phi ee} \equiv g_{B-L}$ when comparing bounds from static EP tests.

The time-varying EP violation caused by a DM ϕ field is related to that in the $B-L$ case by

$$\begin{aligned}\Delta a|_{\phi\bar{e}e,\rm DM} &= y_{\phi ee}\nabla\phi\left(\frac{Z_1}{A_1 m_N} - \frac{Z_2}{A_2 m_N}\right) \\ &\approx \frac{y_{\phi ee} v}{g_{B-L}} \times \Delta a|_{B-L,\rm DM}. \end{aligned} \quad (18)$$

We can therefore use $y_{\phi ee} \equiv g_{B-L}/v$ when comparing the reach of DM searches, with $v \approx 10^{-3}$.

V. EXPERIMENTAL OPTIONS

We consider three ways to measure these EP-violating forces from dark matter. The methods are distinguished by the nature of the test bodies used to perform the measurement. In Sec. V A, we consider torsion pendulums, with laboratory-scale macroscopic masses whose relative accelerations are measured through optical interferometers. In Sec. V B, we consider ballistic atoms as test masses, with their relative accelerations measured through atom interferometry. Finally, in Secs. V C and V D the test masses are celestial objects—the Moon and pulsars. In Sec. V E we summarize our projections and discuss other bounds. Our results are plotted in Figs. 2, 3 and 4. We note that our projections are intended to illustrate the likely reach of future experiments, and neglect details of signal analysis that will have an $\mathcal{O}(1)$ effect on the limits.

A. Torsion Balances

1. Dark matter detection strategy

Torsion balances are currently the most sensitive instruments for measuring static, EP-violating forces [80]. Here we consider using torsion-balance pendulums to detect the time-oscillating, EP-violating forces induced by light bosonic dark matter, as illustrated in Fig. 1.

Torsion balances configured for EP tests carry test bodies of different materials. An EP-violating force would apply different accelerations to the different materials, producing

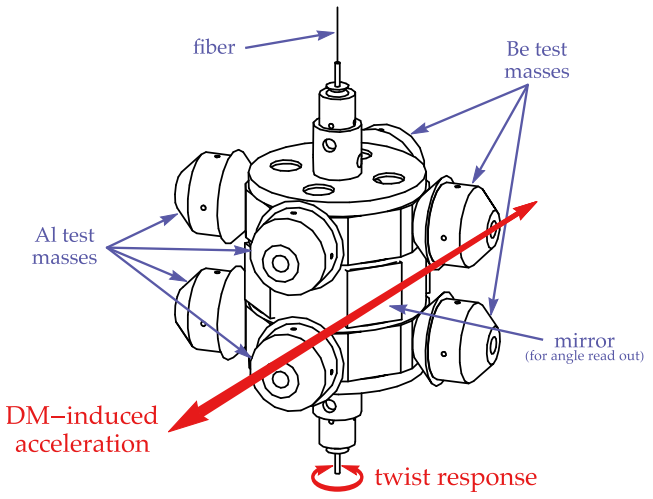

FIG. 1. A torsion pendulum for dark matter direct detection (figure adapted from Ref. [81]). The dark matter field directly induces an equivalence-principle-violating acceleration on the test masses, resulting in an oscillating twist in the pendulum. The twist angle is measured by observing the deflection of a laser reflected from the mirror.

a torque, $\tau(t)$, on the pendulum. The experiment then consists of carefully monitoring the twist angle $\theta(t)$ of the pendulum to infer $\tau(t)$.

In modern experiments, the entire setup is placed on a turntable rotating at a frequency $f_{\rm tt}$. This causes the torque exerted by an otherwise static force to oscillate at this frequency. The DM signal, by contrast, oscillates at a frequency $f_{\rm DM} = m/2\pi$ (the Compton frequency of the DM), modulated by both the turntable frequency $f_{\rm tt}$ and the Earth's rotation frequency $f_\oplus$. Since the DM matter signal does not occur at a frequency associated with either the experiment or the environment, it is naturally distinguishable from most backgrounds.

Torsion balance experiments looking for a static EP-violating force towards the Earth (e.g. Refs. [63,81]) must deal with any effect that produces a pendulum twist at the turntable rotation frequency, such as turntable imperfections, temperature gradients, and gravity gradients. Consider lab-fixed gravity gradients. These apply a torque on the gravitational moments of the pendulum, and the torque changes direction at frequency $f_{\rm tt}$ as the torsion balance rotates, just like a static EP signal. The degree to which one can cancel the gravitational gradients in the lab and the gravitational moments of the pendulum is a limiting factor in these experiments. However, the DM signal always has frequency components separated from $f_{\rm tt}$, even for arbitrarily small DM masses, and so only phase-coherent gravity gradient fluctuations that exactly mimic Eq. (19) affect the measurement. This strategy has been effectively used to suppress the major systematics in searches for sidereally modulated signals in torsion pendulum experiments [82,83], and it should work just as well in searches for the DM modulated signal.

A second major advantage of the DM search over the static search is the direction of the force. The static force sourced by the Earth points in the vertical direction, while a hanging torsion pendulum is sensitive only to horizontal forces. Since the Earth's rotation causes the pendulum to hang at a slight angle, the pendulum is sensitive to the static EP force, but only sensitive at the level of 1 part in 10^3. A DM-induced force, on the other hand, points in a random direction and so avoids this large suppression (note that a DM-induced force points in the insensitive vertical direction at most $\mathcal{O}(50\%)$ of the time, thanks to the rotation of the Earth).

As a result of the turntable rotation and the Earth's rotation, the DM signal occurs at six distinct frequencies,

$$\tau(t) \sim \tau_{\rm DM} \sum_i c_i e^{2\pi i f_i t}, \tag{19}$$

$$f_i = f_{\rm DM} \pm f_{\rm tt} + \left\{ \begin{array}{c} +f_\oplus \\ 0 \\ -f_\oplus \end{array} \right\}, \tag{20}$$

where $f_\oplus$ is the Earth's sidereal (rotation) frequency, as we show in the Appendix. The overall amplitude $\tau_{\rm DM}$ of the induced torque, and the six $\mathcal{O}(1)$ coefficients c_i, are determined by $\Delta\vec{a}_{\rm DM}$, the difference in the DM-induced linear acceleration between the two test materials. This is given in Eqs. (4), (13) and (18) for $B-L$ and scalar DM. In practice one could then fit the $\theta(t)$ data stream to the functional form from Eq. (19), to fully reconstruct the best-fit value of the vector $\Delta\vec{a}_{\rm DM}$ as a function of $f_{\rm DM}$. We elaborate on this briefly in the Appendix, but we postpone studying the details of this analysis to future work. Here we simply take

$$|\tau| \approx \tau_{\rm DM} \approx \frac{1}{2} MR \frac{\Delta a_{\rm DM}}{\sqrt{3}}, \tag{21}$$

where M and R are the combined mass of the test bodies and the arm length of the pendulum. The factor $1/\sqrt{3}$ reflects the fact that only one direction for $\Delta\vec{a}_{\rm DM}$ contributes to the torque at any instant.

2. Noise in torsion balances

We assume statistical noise sources to be the limiting factor in constraining $\Delta a_{\rm DM}$ with torsion balance data. The statistical uncertainty in torsion balance measurements comes from damping noise in the wire, noise in the angle readout, and external sources of noise such as seismic noise or gravity gradient noise. These are described by a noise power $\mathcal{P}_{\Delta a}(f)$, which controls the uncertainty $\sigma_{\Delta a}$ in the measurement of $\Delta a_{\rm DM}$. For an integration time $t_{\rm int} \lesssim 10^6/f_{\rm DM}$, the width of the signal cannot be resolved, and $\sigma_{\Delta a}$ scales as

$$\sigma_{\Delta a}(f) \approx \sqrt{\mathcal{P}_{\Delta a}(f) t_{\rm int}} \quad (f \lesssim 10^6/t_{\rm int}). \tag{22}$$

For longer integration times, when the width of the signal is resolved, $\sigma_{\Delta a}$ can only be improved by performing a bump hunt in $\mathcal{P}_{\Delta a}(f)$, giving

$$\sigma_{\Delta a}(f) \approx 10^3 \sqrt{\mathcal{P}_{\Delta a}(f)/f} (t_{\rm int} f/10^6)^{\frac{1}{4}} \qquad (f \gtrsim 10^6/t_{\rm int}). \tag{23}$$

$\mathcal{P}_{\Delta a}(f)$ is related to the noise power in the pendulum twist, $\mathcal{P}_\theta(f)$, by combining Eq. (21) with the pendulum response function given in Eq. (24),

$$\mathcal{P}_\tau(f) = (2\pi)^4 I^2 ((f^2 - f_0^2)^2 + f_0^4/Q^2) \mathcal{P}_\theta(f), \tag{24}$$

$$\begin{aligned} \mathcal{P}_{\Delta a}(f) &\approx \frac{12}{M^2 R^2} \mathcal{P}_\tau(f) \\ &\approx (2\pi)^4 12 R^2 ((f^2 - f_0^2)^2 + f_0^4/Q^2) \mathcal{P}_\theta(f), \end{aligned} \tag{25}$$

where $2\pi f_0 = \sqrt{\kappa/I}$ is the resonant frequency of the pendulum, $I \approx MR^2$ is the moment of inertia, κ is the

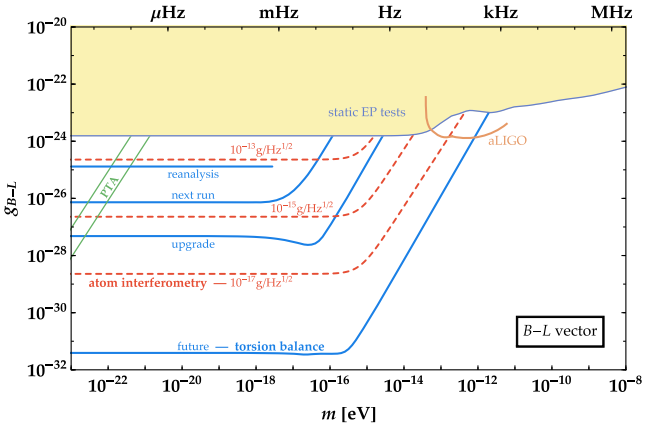

FIG. 2. Estimated reach of searches for $B-L$-coupled vector DM. Solid blue curves correspond to the torsion pendulum setups discussed in Sec. V A. Dashed red curves correspond to atom interferometers with acceleration sensitivities of 10^{-13}, 10^{-15}, and $10^{-18}\,\mathrm{g\,Hz^{-1/2}}$, as discussed in Sec. V B. Thin green curves correspond to the existing EPTA (upper) and upcoming SKA (lower) pulsar timing arrays, as discussed in Sec. V D. The orange curve shows our estimate of the reach of Advanced LIGO, as discussed in Sec. V A 4. The shaded region shows bounds from static EP tests using torsion pendulums [63]. For masses below $\sim 10^{-22}$ eV the field cannot make up all of the dark matter due to its effect on structure formation; this bound may be improved in the future, as discussed in Sec. V E. Additional bounds from black-hole superradiance may apply if the vector has no self interactions, as discussed in Sec. V E. We have not shown estimates for the sensitivity of lunar laser ranging to DM, but even existing data is potentially powerful (see Sec. V C).

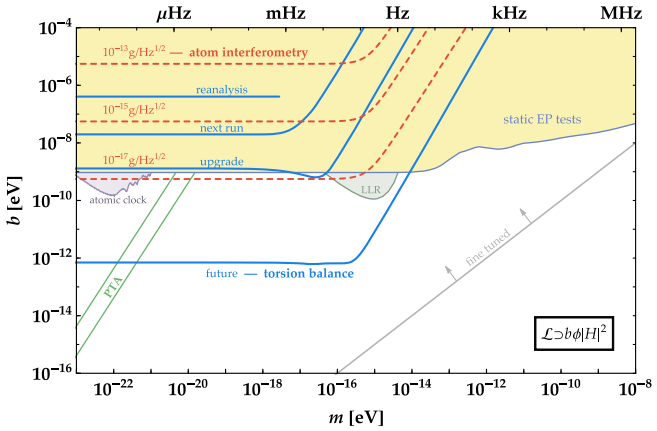

FIG. 3. Estimated reach of searches for scalar DM coupled through the Higgs portal, $\mathcal{L} \supset b\phi|H|^2$. The blue, red and green curves and the yellow shaded region are as in Fig. 2. The shaded green region is excluded by fifth-force constraints from lunar laser ranging [81,84], independent of whether the scalar is DM. The shaded purple region was excluded by the search for scalar DM in atomic clock data [64]. The gray line ($m = b$) shows the approximate boundary above which the scalar mass is fine-tuned. As discussed in Sec. IV C, there is an $\mathcal{O}(1)$ theory uncertainty in the degree of EP violation of the coupling to nuclei, which affects both the static EP-test bounds and the projections for atom interferometer and torsion balance tests.

torsional spring constant, and Q is the quality factor. The f^4 scaling at high frequencies reflects the fact that the twist of the pendulum for a fixed torque drops as $\theta \propto f^{-2}$, since damping becomes irrelevant and the pendulum rotates by the maximum amount possible in a time $1/f$.

Noise $\mathcal{P}_{\theta,\mathrm{r.o.}}$ in the angular readout system limits the sensitivity to an angular deflection of the pendulum. Converting a flat $\mathcal{P}_{\theta,\mathrm{r.o.}}$ spectrum to the corresponding acceleration noise power, using Eqs. (24) and (25), gives a high-frequency scaling

$$\sqrt{\mathcal{P}_{\Delta a,\mathrm{r.o.}}(f)} \approx 3\times 10^{-9}\,\frac{\mathrm{cm\,s^2}}{\sqrt{\mathrm{Hz}}} \times \left(\frac{f}{100\ \mathrm{mHz}}\right)^2 \frac{R}{2\ \mathrm{cm}}\,\frac{\sqrt{\mathcal{P}_{\theta,\mathrm{r.o.}}}}{10^{-9}\ \mathrm{rad\,Hz^{-1/2}}}. \tag{26}$$

This is the limiting factor for the DM sensitivity at high frequencies, as seen in Figs. 2 and 3.

Internal damping in the fiber produces thermal noise in the fiber that dominates the noise of the system at low frequencies. This results in a torque noise $\mathcal{P}_{\tau,\mathrm{th}}(f) = 4T\kappa/(2\pi f Q)$, and an acceleration noise

$$\mathcal{P}_{\Delta a,\mathrm{th}}(f) \approx \frac{48T\kappa}{M^2R^2Q}\frac{1}{2\pi f}. \tag{27}$$

The spring constant κ of the wire scales as $\kappa \propto M^2/L_{\mathrm{wire}}$, where L_{wire} is the length of the wire and M is the maximum mass it can support. The constant of proportionality depends on the wire materials and how it is fabricated. For the 1 m tungsten wire used in the Eöt-Wash setup [63], this gives a noise scaling

$$\sqrt{\mathcal{P}_{\Delta a,\mathrm{th}}(f)} \approx 3\times 10^{-10}\,\frac{\mathrm{cm\,s^2}}{\sqrt{\mathrm{Hz}}} \times \sqrt{\frac{\mathrm{mHz}}{f}}\sqrt{\frac{T}{300\ \mathrm{K}}}\frac{2\ \mathrm{cm}}{R}\sqrt{\frac{5000}{Q}}, \tag{28}$$

where we have normalized to the parameters of the current setup [81] (see Table II). For a fused silica wire, κ and therefore $\mathcal{P}_{\Delta a,\mathrm{th}}$ may be lowered by a factor of ~ 4 compared to tungsten. Using fibers with higher Q or cooling the apparatus to lower temperatures would reduce the effect of thermal noise in the measurement, as would increasing the arm length R (while keeping the active-to-passive mass ratio constant). Torsion pendulums usually have compact (small-R) designs to minimize couplings to gravity gradients. If the time dependence of the DM signal does suppress gravitational gradient-related systematics sufficiently, a larger pendulum can improve the sensitivity to DM at low frequencies. This requires a trade-off with the

TABLE II. Experimental setups assumed for the sensitivity curves labeled "next run," "upgrade" and "future" in Figs. 2,3 and 4. Δ_{B-L} and $\Delta_{\phi|H|^2}$ are the degree of EP violation of a $B-L$ coupled vector and a Higgs-portal coupled scalar, as defined in Eqs. (2) and (14), for the given test-mass combination.

	Test-mass materialstest-mass materials	Δ_{B-L}	$\Delta_{\phi\|H\|^2}$	$\sqrt{P_\theta}$ [rad/$\sqrt{\text{Hz}}$]	R [cm]	M [kg]	Wire material	κ [erg/rad]	Q	T [K]	f_{tt} [mHz]
"next run"	Al/Be	0.037	2×10^{-4}	10^{-9}	2	0.04	Tungsten	0.025	5000	300	10
"upgrade"	Al/Be	0.037	2×10^{-4}	10^{-12}	2	0.04	Fused silica	0.025	10^6	300	10
"future"	$\text{Be}/(\text{C}_3\text{H}_6)_n$	0.13	1×10^{-4}	10^{-18}	16	20.5	Fused silica	1640	10^8	6	100

high-frequency sensitivity, because the effective acceleration noise from the readout system $\mathcal{P}_{\Delta a,\text{r.o.}}(f)$ [Eq. (26)] increases with pendulum size.

As shown in Eq. (28), $\mathcal{P}_{\Delta a,\text{th}}(f)$ gets worse at low frequencies. However, rotating the apparatus boosts low signal frequencies to near f_{tt}, so the noise around f_{tt} limits the experiment for all frequencies below f_{tt}. This is why our sensitivity curves are flat at frequencies below f_{tt}. To optimize the experiment the turntable frequency should, if possible, be at the intersection of the angle readout noise limit (dominating at high frequencies) and the thermal noise limit (dominating at low frequencies). In practice this can be a challenge to achieve. The values of f_{tt} we use in our sensitivity estimates are intended to be realistic, and are slightly below the optimum values.

3. Sensitivity estimates

In Figs. 2, 3 and 4 we show estimated detection sensitivities under four possible scenarios of torsion balance development. For each curve, we show the coupling strength at which dark matter of the given mass would produce a torque on the pendulum equal to the torque noise of the balance, postponing more detailed analysis to future work.

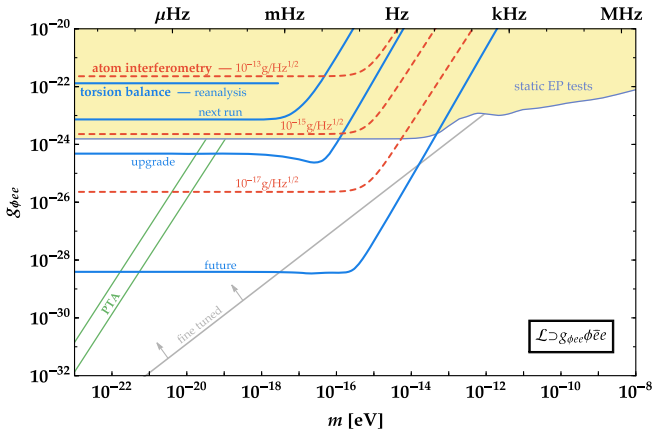

FIG. 4. Estimated reach of searches for scalar DM coupled through $\mathcal{L}\supset g_{\phi ee}\phi\bar{e}e$. The blue, red and green curves and the yellow shaded region are as in Fig. 2. Above the gray line the scalar mass is fine-tuned if the cutoff Λ is above ~TeV.

(1) "reanalysis" is the estimated reach from reanalyzing existing data.
(2) "next run" is based on the continued running of the existing Eöt-Wash setup, with the improved autocollimator described in Ref. [85] and a higher turntable frequency. We assume thermal + readout noise to be the limiting factor.
(3) "upgrade" corresponds to a combination of several upgrades which have been demonstrated in the laboratory but have not yet been implemented in EP experiments, so there is some technical risk.
(4) "future" corresponds to more aggressive upgrades including the use of polypropylene test bodies, including cooling to liquid Helium temperatures and using silica fibers at the limits of the material properties. We also imagine increasing the lever arm of the test bodies by scaling the pendulum up by a factor of 8. This would mean the active and passive masses of the pendulum both increase by 8^3 and would require a very sophisticated angle readout system that reaches the shot noise limit of the system described in Ref. [86]. Other strategies to make larger lever arms have various trade-offs; this is just meant to provide an idea of the reach provided by a larger pendulum. Overall this represents an aggressive projection with significant technology upgrades.

The reanalysis estimate is based on the results of Schlamminger *et al.* [81], where a bound was placed on an EP-violating force that is static in the Galactic frame (equivalent to the $m\to 0$ limit for DM). The limit was $\tau < 10^{-18}$ N m after ~3 years integration time, using a combined Be/Al test mass of 39 g and an arm length of 2 cm, which corresponds to $\Delta a \lesssim 3\times10^{-13}$ cm s^{-2}. We take this value as our estimate, although a reanalysis is required, since even the smallest DM frequencies would shift the signal away from the frequency looked at in Ref. [81].

Table II shows the assumptions we make for the experimental parameters in the other three setups, which we also assume will be limited by thermal and readout noise as described above. Note in particular that it appears possible to improve the angle readout noise of the device significantly. For example in Ref. [86] a sensitivity

of 10^{-12} rad $\mathrm{Hz}^{-\frac{1}{2}}$ was easily achieved with a laser-interferometric setup using an optical lever, so we take this as the "upgrade" readout noise. The shot-noise-limited sensitivity was estimated at 10^{-18} rad $\mathrm{Hz}^{-\frac{1}{2}}$, so we take this as the "future" readout sensitivity. In all cases we assume a 1 year integration time.

The rotating, cryogenic balance assumed for the "future" experiment would be quite a technical feat. However, even without rotating the apparatus these sensitivities could still be achieved for frequencies above ~100 mHz. Below 100 mHz the DM signal is modulated at the sidereal frequency, so the sensitivity would roll off by a factor of 100 between 100 mHz and 10 μHz. It is worth noting that the requirements on the rotation rate uniformity and tilt stabilization of the turntable are somewhat less stringent in searches for the DM signal, since the signal is not at the turntable rotation rate.

4. Comparison with a linear interferometer

If the ultimate limit of such a torsion balance experiment would have a laser-interferometric angle readout system, one can ask whether this torsion pendulum geometry is an improvement over a linear geometry where the two different masses are hung from their own fibers and the linear rather than differential acceleration between them is measured with a laser interferometer.[5] For the linear interferometer the shot noise limit on the displacement sensitivity (in $\frac{\mathrm{m}}{\sqrt{\mathrm{Hz}}}$) is $\sim\frac{\lambda}{\sqrt{N}}$ where λ is the laser wavelength and N is the number of photons per second. The acceleration sensitivity (in $\frac{\mathrm{m}}{\mathrm{s}^2}\frac{1}{\sqrt{\mathrm{Hz}}}$) to an acceleration a with frequency f is then

$$\delta a \sim \frac{\lambda}{\sqrt{N}} f^2. \tag{29}$$

By contrast for the torsion pendulum geometry, the sensitivity is parametrically enhanced over this. The ultimate shot noise limit on angular displacement sensitivity is $\delta\theta \sim \frac{\lambda}{L\sqrt{N}}$ where L is the length of the optical lever arm. The sensitivity to differential linear accelerations of the two proof masses of differing composition is then

$$\delta a \sim \frac{R}{L}\frac{\lambda}{\sqrt{N}} f^2 \tag{30}$$

where R is the radius of the torsion balance. Thus it is enhanced over the linear sensitivity (29) by a factor of $\frac{L}{R}$, the optical lever arm over the size of the torsion balance. So the torsion balance is the optimal geometry for such a signal.

LIGO is an example of a linear interferometer which is very sensitive to accelerations. Advanced LIGO has sensitivity above 10 Hz, with seismic noise eclipsing any lower-frequency signals [87]. The proof masses (mirrors) in LIGO are not made with different materials and so are not designed to search for an EP-violating acceleration. However there is still a signal in LIGO from a DM-induced acceleration, arising *a*) due to its partial oscillation over the light travel time [46], and *b*) due to its spatial gradient, which gives a relative acceleration between the mirrors. This gives an effect which is suppressed by the larger of $(mL)^2$ and mvL, where L is the separation between the mirrors.

Advanced LIGO can probe a region of the $B-L$ vector DM parameter space. We estimate the reach as follows. A DM-induced acceleration, of amplitude a_{DM}, causes the round-trip light travel time (for N bounces between two mirrors) to oscillate with amplitude

$$\delta t_{\mathrm{DM}} \approx \begin{cases} 2Na_{\mathrm{DM}}L^2 & \text{(time variation of DM field)}, \\ 2N\delta L \approx 2N\frac{\Delta a_{\mathrm{DM}}}{\omega^2} \approx 2N\frac{L\partial_x a_{\mathrm{DM}}}{m^2} \approx 2NL\frac{va_{\mathrm{DM}}}{m} & \text{(spatial variation of DM field)}. \end{cases} \tag{31}$$

In comparison, a gravitational wave of amplitude h and frequency $\omega \ll 1/(NL)$ causes the round-trip time to oscillate with amplitude $\delta t_{\mathrm{grav}} \approx 2N\delta L \approx 2NLh$. The DM effect therefore has an effective strain of

$$h_{\mathrm{eff}} \approx \max\left(\frac{10^{-3}}{m}, L\right) \times a_{\mathrm{DM}} \approx \max\left(\frac{10^{-3}}{m}, L\right) \times \frac{g_{B-L}\sqrt{\rho_{\mathrm{DM}}} f_n}{m_N}, \tag{32}$$

where in the last step we have taken the acceleration amplitude for the $B-L$ vector, and $f_n \approx 1/2$ is the neutron fraction of the mirrors.

If LIGO has a strain noise spectral density of S_h, and integrates for time t, then a monochromatic signal could be detected if it has strain $h \gtrsim \sqrt{S_h/t}$. However, this only applies up to the DM coherence time $\tau_{\mathrm{DM}} \approx 10^6/f$; beyond this the finite-frequency spread of the signal is resolved, and the strain sensitivity only improves as $(\tau_{\mathrm{DM}}/t)^{1/4}$. This gives a sensitivity to the DM signal of

$$h_{\mathrm{eff}} \approx \sqrt{S_h}\left(\frac{2\pi m}{10^6 t}\right)^{\frac{1}{4}}. \tag{33}$$

[5]This is similar to one arm of LIGO for example except made much shorter and with test masses of differing composition.

Taking Advanced LIGO's ultimate target noise curve from Ref. [87], and assuming 1 year of integration time, we obtain the estimated reach shown by the orange curve in Fig. 2. The reach for the scalar DM can be similarly estimated, but it does not exceed the static EP bounds, and so we do not show it in Figs. 3 and 4.

B. Atom interferometry

Light pulse atom interferometers [88] have emerged over recent years as precision accelerometers. Currently demonstrated technology is approaching a sensitivity of $\sim 10^{-13}\,\frac{g}{\sqrt{\text{Hz}}}$ at 1 Hz (where $g = 9.8\ \text{ms}^{-2}$), with sensitivities as high as $\sim 10^{-15}\,\frac{g}{\sqrt{\text{Hz}}}$ achievable in the near term, and perhaps $\sim 10^{-17}\,\frac{g}{\sqrt{\text{Hz}}}$ in the further future (perhaps on a time scale of a decade) [89–93]. Experiments to test the equivalence principle using these accelerometers [89,94] are presently under construction [93,95,96]. These experiments operate by dropping colocated clouds of two different atomic species (e.g. Rb-85 and Rb-87) and measuring the differential acceleration between them. In such experiments, since the atom clouds (the test masses) are in free fall during the course of the measurement, the differential acceleration between them is immune to a variety of noise sources such as seismic vibrations and suspension thermal noise that limit conventional optical interferometers, where these noise sources are introduced due to the need to hold the macroscopic proof masses. Atom interferometers face a different set of backgrounds, such as shot noise. As with torsion pendulums, searches for static EP violation may ultimately be limited by gravity gradients. Again as with torsion pendulums, the time oscillation makes the dark matter signal much less susceptible to these, and there exist protocols to reduce backgrounds down to the shot noise floor [91,97] for such AC measurements.

The atom interferometer measures acceleration by sensing the position of the atom clouds at different points in their trajectory. The displacement of the atom clouds scales as t^2, the time over which the acceleration is measured. This time is limited by the free-fall time t_f of the apparatus and the period $1/m$ of the oscillating dark matter signal. To estimate the sensitivity of the atom interferometers, we will take t to be the smaller of these two times. Since the coherence time of the signal is $\sim 10^6/m$, it might be possible to improve over this estimate. For masses $m \gtrsim 1/t_f$, the interferometer could potentially be operated in a resonant mode allowing the displacement to build over several oscillations of the dark matter signal. Similarly, for $m \lesssim 1/t_f$ it might be possible to increase the measurement time by bouncing the atoms many times in the interferometer, effectively increasing the free-fall time. Both of these possibilities deserve further experimental consideration, but we do not include them in our sensitivity estimates.

Under these assumptions, the red curves in Figs. 2, 3 and 4 show our projected sensitivity of atom interferometer searches to an EP-violating dark matter signal. From top to bottom, the curves assume interferometers with acceleration sensitivities of $10^{-13}\,\frac{g}{\sqrt{\text{Hz}}}$, $10^{-15}\,\frac{g}{\sqrt{\text{Hz}}}$, and $10^{-17}\,\frac{g}{\sqrt{\text{Hz}}}$ at 1 Hz. In all cases, the sensitivity drops as $1/f^2$ for frequencies $f > 1$ Hz while remaining flat for frequencies $f < 1$ Hz, consistent with the above assumption about the measurement time. We used Rb-85 and Rb-87 for the atomic species and assumed a total integration time of 10^6 s. These searches are expected to be more powerful than searches for the static EP violation caused by the DM field sourced by the Earth (assuming the field makes up all of the DM).

C. Lunar laser ranging

Lunar laser ranging (LLR) provides a sensitive search for static EP-violating forces. Thus it is worth considering whether it would be useful in the search for this type of oscillating, EP-violating force from dark matter. LLR can detect a new EP-violating force from the Sun that causes a differential acceleration between the Earth and the Moon. Currently the sensitivity is limited by the accuracy of the ranging which is around 1 cm [98]. In order to distinguish the effect of a new force from all the other orbital parameters a fit is performed to the ranging data. A full statistical model is necessary to precisely calculate the expected reach of LLR for our dark matter signal, which is beyond the scope of the paper. Here we give a very rough estimate to motivate a more careful search for DM in LLR data.

The force from dark matter will point in a random direction, uncorrelated with the direction to the Sun or any other objects in the Solar System. This should aid in discriminating it from the effect of other unknown Solar System parameters. Further, it will oscillate in time with a precise frequency which should also aid in discrimination. It is likely that if the period of the dark matter is much shorter than a month, the effect on the Moon's orbit will average down and so the sensitivity will be reduced. But for periods longer than a month (dark matter masses below $\sim 10^{-21}$ eV) the effect should be unsuppressed. If we use the relative (EP-violating) acceleration of the Moon and Earth caused by $B - L$ vector dark matter from Eq. (4) and then multiply by $(1\ \text{month})^2$ we find a rough estimate for the extra distance apart the two are separated by after a month. Requiring this be larger than 1 cm yields a very rough estimate for the sensitivity of LLR to this type of dark matter. This gives a reach in the $B - L$ coupling which is down to $g \sim 5 \times 10^{-26}$ in the mass range below about $\sim 10^{-21}$ eV, about an order of magnitude below current bounds. Of course the real estimate may be better than this since there are already many months worth of data, and the sharp peak in the frequency spectrum of the signal may allow noise to be removed. It would thus be very interesting

to reanalyze the LLR data to search for this dark matter signal.

D. Pulsar timing arrays

Observational constraints permit the mass of the dark matter to be as low as $m \sim 10^{-22}$ eV, leading to oscillating effects with periods as long as ∼year. Celestial test bodies offer a powerful way to probe signals at these ultralow frequencies. In particular, leveraging the exceptional stability of pulsars, timing arrays that measure differences in the arrival times of signals from a number of pulsars have been proposed as a way to search for gravitational waves in the $\sim 10^{-8}$–10^{-6} Hz frequency band [99,100]. These pulsar timing arrays are automatically sensitive to the ultralight bosonic dark matter considered in this paper.

One possible signal, considered in Refs. [101,102], arises due to the purely gravitational effect the oscillating dark matter field has on the metric. This may be possible to observe for the lowest DM masses, but the signal falls rapidly to unobservable levels at higher masses (with no other free model parameter to compensate). However, much larger effects can arise due to the direct couplings of the dark matter field to ordinary matter. In the case of the scalar dark matter, the strongest effect arises directly in the timing measurements, which are made using atomic clocks. The oscillation of the scalar field causes the electron mass to oscillate, as discussed in Sec. III. This causes the timing of all terrestrial clocks to oscillate with the same fractional magnitude, since atomic clock frequencies are set by the spacings between atomic energy levels which are proportional to the electron mass. Of course, the pulsars "clocks" are also affected by the scalar field oscillations. For example the neutron mass also changes and this will affect the moment of inertia of the pulsar and hence its spin rate. However, the pulsars being observed are far enough from the Earth that they are all well beyond the Compton wavelength of even the lightest possible dark matter candidate. Therefore the observed effect on the timing for each pulsar is $\mathcal{O}(1)$ different from the effect on terrestrial atomic clocks, and also $\mathcal{O}(1)$ different from the effect on every other pulsar (and does not rely on the EP violation of the force). Averaging many pulsars together then essentially provides a stable definition of time where the dark matter effect averages to zero (or more precisely is reduced by the square root of the number of pulsars). This definition of time is then compared to terrestrial atomic clocks which have oscillations in their timing caused by the dark matter. This is conceptually similar to a comparison between different atomic clocks [46,64], although here the pulsars provide a standard of time to compare to which essentially does not oscillate with the dark matter. This gives a timing residual of

$$\Delta t = t_{\rm clock} - t = \int dt \frac{\omega_{\rm clock}(t)}{\omega_{\rm clock,0}} - t \approx \frac{1}{m}\left|\frac{\delta m_e}{m_e}\right| \sin mt. \tag{34}$$

For the Higgs-portal scalar coupling, $|\delta m_e/m_e| \approx b\sqrt{\rho_{\rm DM}}/(m m_h^2)$, while for a scalar coupled to the electron mass $|\delta m_e/m_e| \approx g_{\phi ee}\sqrt{\rho_{\rm DM}}/(m m_e)$. This signal is observable in pulsar timing arrays in a similar way to a gravitational wave.

We estimate the sensitivity to scalar dark matter of the existing European Pulsar Timing Array (EPTA), and of 10 years of running of the upcoming Square Kilometer Array (SKA) [103], by comparing the maximum timing residual to the timing sensitivity of the array. From Ref. [104], this sensitivity is $\Delta t \approx \sigma_t/\sqrt{N_p N_m}$, where $\sigma_t \sim$ 100 ns (30 ns), $N_p = 5$ (50) is the number of pulsars, and $N_m = 10\ \mathrm{yr}/2$ weeks is the number of measurements per pulsar. (This is approximately equivalent to equating the maximum fractional change of m_e to the gravitational-wave strain sensitivity estimated in Ref. [100].) We show our estimates of these sensitivities in Figs. 3 and 4.

Dark matter also gives rise to a timing residual due to the force it exerts on matter. This results in a physical displacement of both the Earth and pulsars, which as before are not in phase with each other due to the large separation lengths, resulting in an observed timing residual (again this does not rely on the EP violation of the force, which anyway is relatively large). For the Higgs-coupled scalar, this effect is $\mathcal{O}(10^{-4})$ smaller than the dilation effect due to the velocity suppression of the force, and the smaller fractional coupling of the scalar to the nucleon mass than the electron mass. For the $B - L$ coupled vector it gives the dominant effect, resulting in a timing residual of

$$\Delta t = \Delta x = \frac{a}{m^2} \approx \frac{g_{B-L}\sqrt{\rho_{\rm DM}}}{2\sqrt{3} m_n m^2} \tag{35}$$

where the factor of 2 accounts for the fact that the Earth is ∼50% neutrons, and the factor of $\sqrt{3}$ accounts for the fact that we only observe displacements along the line of sight to a given pulsar. Comparing to the timing sensitivity discussed above gives the estimated sensitivity shown in Fig. 2.

Both the time-dilation signal and the acceleration signal are similar to a gravitational-wave signal in a pulsar timing array, with the key difference that these signals are not tensor in nature (they are scalar and vector in nature respectively). A gravitational wave causes contraction along one axis and expansion in a perpendicular axis, and thus the timing changes from pulsars depend on the direction to the pulsar in this tensorial manner. However in the case of scalar dark matter, the timing change is describable just as a change to terrestrial atomic clocks and is therefore independent of the direction to the comparison pulsar. For an acceleration signal, the Earth accelerates in a particular direction. Thus the timing changes to pulsars in that direction have one sign, the timing changes to pulsars in the opposite direction along the same axis have a different sign, and there is no timing

change to pulsars in the two perpendicular directions. While such scalar and vector signals are certainly visible to pulsar timing arrays, searching for them likely requires a slightly different analysis than the gravitational-wave analysis. It would thus be interesting for the pulsar timing arrays to undertake searches for scalar and vector signals.

E. Projected sensitivities

In Figs. 2,3 and 4 we show our estimated sensitivities for the various torsion pendulum, atom interferometer, and pulsar timing array setups discussed above. We emphasize that the upper curves for the torsion pendulum and pulsar timing array correspond to possible reanalyses of existing data. In all three cases the lowest curves are expected to be reachable in the time scale of a decade. We note that all lines in Fig. 3 assume the EP violation given by and directly below Eq. (14). This neglects $\mathcal{O}(1)$ uncertainties in these parameters, as discussed in Sec. IV C.

As can be seen from the plots, there is significant potential to probe untested DM parameter space, most dramatically in the case of $B-L$ vector DM or a scalar DM coupled to the electron mass.

Existing constraints We also show several existing constraints. The yellow shaded regions show bounds from static EP tests using torsion pendulums [63]. We converted these bounds from the $B-L$ case into the scalar cases according the formulas given in Secs. IV C and IV D. The green shaded region in Fig. 3 labeled LLR shows the bound from tests of the gravitational inverse-square law using lunar laser ranging [81,84]. In Figs. 2 and 4 these bounds are weaker than the static EP bounds and so do not appear. The static EP and lunar laser ranging bounds arise due to the light field being sourced by the Earth, and are independent of the field's contribution to dark matter.

The light purple shaded region in Fig. 3 shows the bound from a search for scalar dark matter in atomic clock data [64] appearing as an oscillating change to α. We converted these into bounds on b assuming a coupling $\mathcal{L} \supset (g_{h\gamma\gamma} b/m_h^2)\phi F_{\mu\nu}F^{\mu\nu}$, with $g_{h\gamma\gamma} \approx \alpha/8\pi$ [62]. Dedicated atomic clock searches may have significantly increased sensitivity to scalar dark matter in the future [46]. The gray lines in Figs. 3 and 4 mark the edge of the natural region (assuming a cutoff above ~TeV in the electron-coupled case); the parameter space to the left requires fine-tuning.

Other potential signatures In addition to the signatures and constraints already discussed, there are two other potential signatures of ultralight DM which do not appear on our plots but are worth mentioning. First, the effect that ultralight bosonic DM has on structure formation may be observable for masses above the currently estimated lower mass limit of $\sim 10^{-22}$ eV. It has been estimated that, with improved structure formation modeling, future cosmic microwave background and 21 cm observations may probe DM masses as large as $\sim 10^{-18}$ eV [8,10].

Second, the existence of a light bosonic field can allow spinning black holes to rapidly lose angular momentum through "superradiance" [53–56,105]. The existence of rapidly spinning black holes therefore constrains such new light bosons, with current black hole measurements excluding a range of masses around 10^{-12}–10^{-11} and 10^{-17}–10^{-16} eV [55]. However, these bounds assume gravitational interactions only, and disappear if the new field has small self-interactions [53]. We therefore do not show these bounds in our plots, since the fields we consider may well have such self-interactions (in fact, for the scalars, we find that their couplings to the Standard Model guarantee this in the entire experimentally accessible region).

VI. CONCLUSIONS

Ultra-weakly coupled, light bosonic particles emerge in a number of theories of physics beyond the Standard Model, and are an important target for experimental searches. They may play an important role in resolving major problems in particle physics such as the strong CP problem, the electroweak hierarchy problem [57], and possibly the cosmological constant problem [106]. In these approaches, the solutions to these outstanding problems are not the result of high-energy physics but rather the product of low-energy dynamics. If these fields exist, it is natural for them to be dark matter. It is important to pursue the experimental signatures of these alternative possibilities. The ultralight mass range, where dark matter behaves as a coherent oscillating classical field, spans over 20 orders of magnitude in mass from $\sim 10^{-22}$ eV to ~eV. Masses at the lowest end may help resolve potential problems with small-scale structure [6,107]. Here, we have proposed probes of the lighter half of this parameter space, using sensitive measurements of time-dependent, EP-violating accelerations. Existing accelerometers are already sensitive to new parameter space, and we project that near-future technology will improve bounds up to 10 orders of magnitude in coupling strength.

Quantum field theory restricts the ways in which a particle can be naturally light to a small number of leading possibilities, such as derivative interactions (such as axions), kinetic mixing with electromagnetism, minimal gauge couplings, and the Higgs portal. There are a variety of experiments that source and detect these particles in the laboratory, such as experiments that search for spin-dependent forces (for axions [70–73]), the transmission of electromagnetic radiation through a shield (for kinetically mixed hidden photons [31,39]) and experiments that search for new short-distance/equivalence-principle-violating forces between test bodies [89,108,109]. The other option besides experiments that both source and detect these particles is to search for an existing cosmic abundance of such particles. There have been a handful of ideas of how to discover these new fields if they make up the dark matter.

The effects discussed in Sec. III encompass *all* the experimental avenues to directly search for the interactions of ultralight dark matter. A variety of experimental avenues to search for the time-dependent signals caused by a cosmic abundance of axions and hidden photons are currently being pursued, while there are no experiments designed to search for the time-varying accelerations caused by $B-L$ gauge bosons and scalars (such a relaxion). We can search for ultralight dark matter through its effects on photons, electrons and nucleons. Presently, microwave cavities [21] (and potentially, LC resonators [110,111]) are used to search for axions through their mixing with photons. Scalar dark matter coupling to photons or fermions can cause oscillations of fundamental parameters of the Standard Model, which may be searched for using atomic clocks [46,64] or possibly resonant bars [47]. The effects of dark matter on fermions such as electrons and nucleons fall into two broad categories: the dark matter can lead to precession of their spins (the target of the CASPEr experiment [25,26]) or lead to forces acting on them. Of the many possible kinds of forces, there is one particular combination that is aligned with electromagnetism (the hidden photon) and this force can be searched for using LC resonator experiments [41]. Any other type of force will result in an equivalence-principle-violating acceleration of electrically neutral atoms. The phenomenology will thus be similar to the concepts discussed in this paper.

In this paper we have proposed experimental searches for a cosmic abundance of ultralight vectors or scalars using precision accelerometers. Such light field dark matter may generically exert direct, time-oscillating, EP-violating forces on normal matter. These give rise to accelerations, resulting in the displacement of test bodies that can be measured with torsion pendulums, atom interferometers and pulsar timing arrays. Since this displacement scales as m^{-2}, an acceleration signal that has a fixed magnitude (such as the signal from dark matter) leads to a larger measurable displacement signal at lower frequencies/masses. Since accelerometers appear to be ill suited to search for high-frequency signals, it would be interesting to develop alternate protocols that can probe these high-frequency regions. The EP-violating nature of the dark matter signal enables its detection in compact laboratory setups, since there is a no need for a long baseline. This suppresses backgrounds such as time-varying gravity gradient noise and seismic vibration noise that normally plague long-baseline accelerometer setups such as terrestrial gravitational-wave detectors. Removing these backgrounds makes it possible to search for low-frequency signals, where accelerometer sensitivity is maximized. Thus, accelerometers such as torsion pendulums and atom interferometers are optimal ways to directly detect such light dark matter over 10 orders of magnitude in mass from $\sim 10^{-8}$ Hz to kHz. The searches we have proposed can probe new parameter space with existing technology, and should push many orders of magnitude further in coupling with expected technology upgrades over the coming years. Our present proposals help establish a full experimental program to discover light dark matter.

ACKNOWLEDGMENTS

We would like to thank E. Adelberger, S. Dimopoulos, R. Harnik, J. Hogan, A. Sushkov, K. Van Tilburg. P. W. G. acknowledges the support of NSF Grant No. PHY-1316706, DOE Early Career Award No. DE-SC0012012, and the W. M. Keck Foundation. S. R. was supported in part by the NSF under Grants No. PHY-1417295 and No. PHY-1507160, the Simons Foundation Award No. 378243. D. E. K. acknowledges the support of NSF Grant No. PHY-1214000. This work was supported in part by the Heising-Simons Foundation Grants No. 2015-037 and No. 2015-038.

APPENDIX: DM SIGNAL IN A ROTATING TORSION BALANCE

In this appendix we derive and discuss the form of the signal in a rotating pendulum arising due to a DM-induced acceleration that is fixed in the Galactic rest frame. The result is of importance for discriminating a DM signal from backgrounds: the signal has a distinctive pattern, with six different frequencies with correlated phases and amplitudes.

(i) Let $\{\hat{x}_\oplus, \hat{y}_\oplus, \hat{z}_\oplus\}$ define coordinates for an observer standing on the Earth, chosen so that $\hat{z}_\oplus$ is the axis of the Earth's rotation, and $\hat{y}_\oplus$ is east. Since these coordinates rotate with the Earth, a vector $\vec{E}$ that is not rotating with the Earth has the form

$$\begin{aligned}\vec{E}(t) = {} & E_1(t)(\cos(2\pi f_\oplus t)\hat{x}_\oplus - \sin(2\pi f_\oplus t)\hat{y}_\oplus) \\ & + E_2(t)(\sin(2\pi f_\oplus t)\hat{x}_\oplus + \cos(2\pi f_\oplus t)\hat{y}_\oplus) \\ & + E_3(t)\hat{z}_\oplus, \end{aligned} \tag{A1}$$

where $f_\oplus = 4.84 \times 10^{-6}$ Hz is the Earth's rotation frequency.

(ii) In a lab at latitude α, let $\{\hat{x}_{\rm lab}, \hat{y}_{\rm lab}, \hat{z}_{\rm lab}\}$ point south, east, and upwards respectively. Then then $\hat{y}_{\rm lab} = \hat{y}_\oplus$ and $\hat{x}_{\rm lab} = \sin\alpha\hat{x}_\oplus - \cos\alpha\hat{z}_\oplus$.

(iii) A torsion pendulum on a horizontal rotating turntable feels a torque from the azimuthal component of $\vec{E}$, i.e. the component along the direction $\hat{\theta} = \sin(2\pi f_{\rm tt}t)\hat{x}_{\rm lab} - \cos(2\pi f_{\rm tt}t)\hat{y}_{\rm lab}$, where $f_{\rm tt}$ is the turntable frequency. This is given by

$$\begin{aligned} E_\theta(t) = {} & E_1(t)(\sin\alpha\cos(2\pi f_\oplus t)\sin(2\pi f_{\rm tt}t) \\ & + \sin(2\pi f_\oplus t)\cos(2\pi f_{\rm tt}t)) \\ & + E_2(t)(\sin\alpha\sin(2\pi f_\oplus t)\sin(2\pi f_{\rm tt}t) \\ & - \cos(2\pi f_\oplus t)\cos(2\pi f_{\rm tt}t)) \\ & - E_3(t)\cos\alpha\sin(2\pi f_{\rm tt}t). \end{aligned} \tag{A2}$$

(iv) If $\vec{E}(t)$ has frequency $f_{\rm DM}$ in the Galactic frame, there will therefore be signals in the torsion pendulum at six different frequencies:

$$f_{\rm obs} = \left| f_{\rm DM} \pm f_{\rm tt} + \left\{ \begin{array}{c} +f_\oplus \\ 0 \\ -f_\oplus \end{array} \right\} \right|. \qquad \text{(A3)}$$

As discussed in Sec. VA, this splitting pattern is a distinctive signature of the extraterrestrial origin of the signal, and so will be a useful test of a DM signal. It can be resolved as long as $f_\oplus \gtrsim \Delta f_{\rm DM} \approx 10^{-6} f_{\rm DM}$, i.e. $f_{\rm DM} \lesssim 0.5$ Hz, and as long as the integration time is longer than $\sim$1 day (although it will compete with systematics which modulate daily). It will also reduce the backgrounds for the extremely low-mass DM, since a static gravity gradient or a turntable imperfection appears as signals at frequency $f_{\rm tt}$, while a DM signal has components shifted from this by at least $f_\oplus$.

Since there are six signal frequencies (12 real parameters) but only three components of $\vec{E}$ (six real parameters), there are correlations between the amplitudes and phases of the different frequency components. In principle this allows the full (complex) vector $\vec{E}$ to be determined, and the remaining constraints provide further checks of the signal. For $B-L$ vector DM, E_1, E_2 and E_3 are expected to be uncorrelated and have the same rms amplitude. For scalar DM, $\vec{E}$ is replaced with $\vec{\nabla}\phi$, which is expected to point on average in the direction of the Earth's motion. This difference should ultimately allow the two cases to be distinguished.

[1] D. Clowe, M. Bradac, A. H. Gonzalez, M. Markevitch, S. W. Randall, C. Jones, and D. Zaritsky, A direct empirical proof of the existence of dark matter, Astrophys. J. **648**, L109 (2006).

[2] P. Ade *et al.* (Planck Collaboration), Planck 2015 Results. XIII. Cosmological parameters, arXiv:1502.01589.

[3] M. Khlopov, B. A. Malomed, and I. B. Zeldovich, Gravitational instability of scalar fields and formation of primordial black holes, Mon. Not. R. Astron. Soc. **215**, 575 (1985).

[4] W. H. Press, B. S. Ryden, and D. N. Spergel, Single Mechanism for Generating Large Scale Structure and Providing Dark Missing Matter, Phys. Rev. Lett. **64**, 1084 (1990).

[5] V. Sahni and L.-M. Wang, A new cosmological model of quintessence and dark matter, Phys. Rev. D **62**, 103517 (2000).

[6] W. Hu, R. Barkana, and A. Gruzinov, Cold and Fuzzy Dark Matter, Phys. Rev. Lett. **85**, 1158 (2000).

[7] R. Hlozek, D. Grin, D. J. Marsh, and P. G. Ferreira, A search for ultralight axions using precision cosmological data, Phys. Rev. D **91**, 103512 (2015).

[8] B. Bozek, D. J. E. Marsh, J. Silk, and R. F. G. Wyse, Galaxy UV-luminosity function and reionization constraints on axion dark matter, Mon. Not. R. Astron. Soc. **450**, 209 (2015).

[9] H.-Y. Schive, T. Chiueh, T. Broadhurst, and K.-W. Huang, Contrasting galaxy formation from quantum wave dark matter, ψDM, with ΛCDM, using Planck and Hubble data, Astrophys. J. **818**, 89 (2016).

[10] D. J. E. Marsh, Nonlinear hydrodynamics of axion dark matter: Relative velocity effects and quantum forces, Phys. Rev. D **91**, 123520 (2015).

[11] M. W. Goodman and E. Witten, Detectability of certain dark matter candidates, Phys. Rev. D **31**, 3059 (1985).

[12] F. Wilczek, Problem of Strong P and T Invariance in the Presence of Instantons, Phys. Rev. Lett. **40**, 279 (1978).

[13] S. Weinberg, A New Light Boson?, Phys. Rev. Lett. **40**, 223 (1978).

[14] R. D. Peccei and H. R. Quinn, CP Conservation in the Presence of Instantons, Phys. Rev. Lett. **38**, 1440 (1977).

[15] M. Dine and W. Fischler, The not so harmless axion, Phys. Lett. B **120**, 137 (1983).

[16] J. Preskill, M. B. Wise, and F. Wilczek, Cosmology of the invisible axion, Phys. Lett. B **120**, 127 (1983).

[17] L. Abbott and P. Sikivie, A cosmological bound on the invisible axion, Phys. Lett. B **120**, 133 (1983).

[18] D. S. Akerib *et al.* (LUX Collaboration), Improved WIMP scattering limits from the LUX experiment, arXiv:1512.03506.

[19] J. Abdallah *et al.*, Simplified models for dark matter searches at the LHC, Phys. Dark Univ. **9–10**, 8 (2015).

[20] P. Sikivie, Experimental Tests of the Invisible Axion, Phys. Rev. Lett. **51**, 1415 (1983); **52**, 695(E) (1984).

[21] S. Asztalos *et al.* (ADMX Collaboration), A SQUID-Based Microwave Cavity Search for Dark-Matter Axions, Phys. Rev. Lett. **104**, 041301 (2010).

[22] S. Asztalos *et al.* (ADMX Collaboration), Design and performance of the ADMX SQUID-based microwave receiver, Nucl. Instrum. Methods Phys. Res., Sect. A **656**, 39 (2011).

[23] A. Arvanitaki, S. Dimopoulos, S. Dubovsky, N. Kaloper, and J. March-Russell, String axiverse, Phys. Rev. D **81**, 123530 (2010).

[24] P. W. Graham and S. Rajendran, Axion dark matter detection with cold molecules, Phys. Rev. D **84**, 055013 (2011).

[25] P. W. Graham and S. Rajendran, New observables for direct detection of axion dark matter, Phys. Rev. D **88**, 035023 (2013).

[26] D. Budker, P. W. Graham, M. Ledbetter, S. Rajendran, and A. Sushkov, Proposal for a Cosmic Axion Spin Precession Experiment (CASPEr), Phys. Rev. X **4**, 021030 (2014).

[27] A. Arvanitaki and A. A. Geraci, Resonantly Detecting Axion-Mediated Forces with Nuclear Magnetic Resonance, Phys. Rev. Lett. **113**, 161801 (2014).
[28] J. E. Kim and D. J. E. Marsh, An ultralight pseudoscalar boson, Phys. Rev. D **93**, 025027 (2016).
[29] D. J. E. Marsh, Axion cosmology, arXiv:1510.07633.
[30] M. Ahlers, H. Gies, J. Jaeckel, J. Redondo, and A. Ringwald, Light from the hidden sector, Phys. Rev. D **76**, 115005 (2007).
[31] J. Jaeckel and A. Ringwald, A cavity experiment to search for hidden sector photons, Phys. Lett. B **659**, 509 (2008).
[32] R. Povey, J. Hartnett, and M. Tobar, Microwave cavity light shining through a wall optimization and experiment, Phys. Rev. D **82**, 052003 (2010).
[33] A. E. Nelson and J. Scholtz, Dark light, dark matter and the misalignment mechanism, Phys. Rev. D **84**, 103501 (2011).
[34] P. Arias, D. Cadamuro, M. Goodsell, J. Jaeckel, J. Redondo, and A. Ringwald, Wispy cold dark matter, J. Cosmol. Astropart. Phys. 06 (2012) 013.
[35] D. Horns, J. Jaeckel, A. Lindner, A. Lobanov, J. Redondo, and A. Ringwald, Searching for wispy cold dark matter with a dish antenna, J. Cosmol. Astropart. Phys. 04 (2013) 016.
[36] H. An, M. Pospelov, and J. Pradler, Dark Matter Detectors as Dark Photon Helioscopes, Phys. Rev. Lett. **111**, 041302 (2013).
[37] S. R. Parker, G. Rybka, and M. E. Tobar, Hidden sector photon coupling of resonant cavities, Phys. Rev. D **87**, 115008 (2013).
[38] M. Betz, F. Caspers, M. Gasior, M. Thumm, and S. Rieger, First results of the CERN Resonant Weakly Interacting sub-eV Particle Search (CROWS), Phys. Rev. D **88**, 075014 (2013).
[39] P. W. Graham, J. Mardon, S. Rajendran, and Y. Zhao, A parametrically enhanced hidden photon search, Phys. Rev. D **90**, 075017 (2014).
[40] P. Arias, A. Arza, B. Dbrich, J. Gamboa, and F. Mendez, Extracting hidden-photon dark matter from an LC-circuit, Eur. Phys. J. C **75**, 310 (2015).
[41] S. Chaudhuri, P. W. Graham, K. Irwin, J. Mardon, S. Rajendran, and Y. Zhao, A radio for hidden-photon dark matter detection, Phys. Rev. D **92**, 075012 (2015).
[42] H. An, M. Pospelov, J. Pradler, and A. Ritz, Direct detection constraints on dark photon dark matter, Phys. Lett. B **747**, 331 (2015).
[43] P. W. Graham, J. Mardon, and S. Rajendran, Vector dark matter from inflationary fluctuations, Phys. Rev. D **92**, 075012 (2015).
[44] M. Pospelov, S. Pustelny, M. P. Ledbetter, D. F. J. Kimball, W. Gawlik, and D. Budker, Detecting Domain Walls of Axionlike Models Using Terrestrial Experiments, Phys. Rev. Lett. **110**, 021803 (2013).
[45] A. Derevianko and M. Pospelov, Hunting for topological dark matter with atomic clocks, Nat. Phys. **10**, 933 (2014).
[46] A. Arvanitaki, J. Huang, and K. Van Tilburg, Searching for dilaton dark matter with atomic clocks, Phys. Rev. D **91**, 015015 (2015).
[47] A. Arvanitaki, S. Dimopoulos, and K. Van Tilburg, The Sound of Dark Matter: Searching for Light Scalars with Resonant-Mass Detectors, Phys. Rev. Lett. **116**, 031102 (2016).
[48] E. Izaguirre, G. Krnjaic, and M. Pospelov, Probing new physics with underground accelerators and radioactive sources, Phys. Lett. B **740**, 61 (2015).
[49] Y. V. Stadnik and V. V. Flambaum, Axion-induced effects in atoms, molecules, and nuclei: Parity nonconservation, anapole moments, electric dipole moments, and spin-gravity and spin-axion momentum couplings, Phys. Rev. D **89**, 043522 (2014).
[50] Y. V. Stadnik and V. V. Flambaum, Nuclear spin-dependent interactions: Searches for WIMP, axion and topological defect dark matter, and tests of fundamental symmetries, Eur. Phys. J. C **75**, 110 (2015).
[51] Y. V. Stadnik and V. V. Flambaum, Searching for Dark Matter and Variation of Fundamental Constants with Laser and Maser Interferometry, Phys. Rev. Lett. **114**, 161301 (2015).
[52] Y. V. Stadnik and V. V. Flambaum, Enhanced effects of variation of the fundamental constants in laser interferometers and application to dark matter detection, arXiv:1511.00447.
[53] A. Arvanitaki and S. Dubovsky, Exploring the string axiverse with precision black hole physics, Phys. Rev. D **83**, 044026 (2011).
[54] P. Pani, V. Cardoso, L. Gualtieri, E. Berti, and A. Ishibashi, Black Hole Bombs and Photon Mass Bounds, Phys. Rev. Lett. **109**, 131102 (2012).
[55] A. Arvanitaki, M. Baryakhtar, and X. Huang, Discovering the QCD axion with black holes and gravitational waves, Phys. Rev. D **91**, 084011 (2015).
[56] R. Brito, V. Cardoso, and P. Pani, Superradiance, Lect. Notes Phys. **906**, 1 (2015).
[57] P. W. Graham, D. E. Kaplan, and S. Rajendran, Cosmological Relaxation of the Electroweak Scale, Phys. Rev. Lett. **115**, 221801 (2015).
[58] R. L. Davis, Cosmic axions from cosmic strings, Phys. Lett. B **180**, 225 (1986).
[59] S. Chang, C. Hagmann, and P. Sikivie, Studies of the motion and decay of axion walls bounded by strings, Phys. Rev. D **59**, 023505 (1998).
[60] D. Horns, A. Lindner, A. Lobanov, and A. Ringwald, WISP dark matter eXperiment and prospects for broadband dark matter searches in the 1 μeV–10 meV mass range, in *Proceedings, 10th Patras Workshop on Axions, WIMPs and WISPs (AXION-WIMP 2014): Geneva, Switzerland, June 29–July 4, 2014*, edited by E. Tsesmelis and M. Maroudas (DESY, Hamburg, 2014).
[61] J. Suzuki, T. Horie, Y. Inoue, and M. Minowa, Experimental search for hidden photon CDM in the eV mass range with a dish antenna, J. Cosmol. Astropart. Phys. 09 (2015) 042.
[62] F. Piazza and M. Pospelov, Sub-eV scalar dark matter through the super-renormalizable Higgs portal, Phys. Rev. D **82**, 043533 (2010).
[63] T. A. Wagner, S. Schlamminger, J. H. Gundlach, and E. G. Adelberger, Torsion-balance tests of the weak equivalence principle, Classical Quantum Gravity **29**, 184002 (2012).

[64] K. Van Tilburg, N. Leefer, L. Bougas, and D. Budker, Search for Ultralight Scalar Dark Matter with Atomic Spectroscopy, Phys. Rev. Lett. **115**, 011802 (2015).
[65] N. Arkani-Hamed, H. Georgi, and M. D. Schwartz, Effective field theory for massive gravitons and gravity in theory space, Ann. Phys. (Amsterdam) **305**, 96 (2003).
[66] C. de Rham, Massive gravity, Living Rev. Relativity **17**, 7 (2014).
[67] S. L. Dubovsky, P. G. Tinyakov, and I. I. Tkachev, Massive Graviton as a Testable Cold Dark Matter Candidate, Phys. Rev. Lett. **94**, 181102 (2005).
[68] H.-Y. Schive, T. Chiueh, and T. Broadhurst, Cosmic structure as the quantum interference of a coherent dark wave, Nat. Phys. **10**, 496 (2014).
[69] H.-Y. Schive, M.-H. Liao, T.-P. Woo, S.-K. Wong, T. Chiueh, T. Broadhurst, and W. Y. P. Hwang, Understanding the Core-Halo Relation of Quantum Wave Dark Matter from 3D Simulations, Phys. Rev. Lett. **113**, 261302 (2014).
[70] J. E. Moody and F. Wilczek, New macroscopic forces?, Phys. Rev. D **30**, 130 (1984).
[71] J. M. Brown, S. J. Smullin, T. W. Kornack, and M. V. Romalis, A new limit on Lorentz- and *CPT*-violating neutron spin interactions, in *CPT and Lorentz Symmetry*, edited by V. A. Kostelecký (World Scientific, Singapore, 2010), p. 75.
[72] B. R. Heckel, W. A. Terrano, and E. G. Adelberger, Limits on Exotic Long-Range Spin-Spin Interactions of Electrons, Phys. Rev. Lett. **111**, 151802 (2013).
[73] W. A. Terrano, E. G. Adelberger, J. G. Lee, and B. R. Heckel, Short-Range, Spin-Dependent Interactions of Electrons: A Probe for Exotic Pseudo-Goldstone Bosons, Phys. Rev. Lett. **115**, 201801 (2015).
[74] R. Bhre *et al.*, Any light particle search II—Technical design report, J. Instrum. **8**, T09001 (2013).
[75] J. Harms, Terrestrial gravity fluctuations, Living Rev. Relativity **18**, 3 (2015).
[76] E. G. Adelberger, J. H. Gundlach, B. R. Heckel, S. Hoedl, and S. Schlamminger, Torsion balance experiments: A low-energy frontier of particle physics, Prog. Part. Nucl. Phys. **62**, 102 (2009).
[77] S. Durr *et al.*, Lattice Computation of the Nucleon Scalar Quark Contents at the Physical Point, arXiv:1510.08013 [Phys. Rev. Lett. (to be published)].
[78] J. M. Alarcon, L. S. Geng, J. Martin Camalich, and J. A. Oller, The strangeness content of the nucleon from effective field theory and phenomenology, Phys. Lett. B **730**, 342 (2014).
[79] S. R. Beane, S. D. Cohen, W. Detmold, H. W. Lin, and M. J. Savage, Nuclear σ terms and scalar-isoscalar WIMP-nucleus interactions from lattice QCD, Phys. Rev. D **89**, 074505 (2014).
[80] A. M. Nobili, G. L. Comandi, R. Pegna, D. Bramanti, S. Doravari, F. Maccarone, and D. M. Lucchesi, Testing the weak equivalence principle, in *Relativity in Fundamental Astronomy: Dynamics, Reference Frames, and Data Analysis*, edited by S. A. Klioner, P. K. Seidelmann, and M. H. Soffel (Cambridge, University Press, Cambridge, England, 2010), p. 390.
[81] S. Schlamminger, K. Y. Choi, T. A. Wagner, J. H. Gundlach, and E. G. Adelberger, Test of the Equivalence Principle Using a Rotating Torsion Balance, Phys. Rev. Lett. **100**, 041101 (2008).
[82] Y. Su, B. R. Heckel, E. G. Adelberger, J. H. Gundlach, M. Harris, G. L. Smith, and H. E. Swanson, New tests of the universality of free fall, Phys. Rev. D **50**, 3614 (1994).
[83] B. R. Heckel, E. G. Adelberger, C. E. Cramer, T. S. Cook, S. Schlamminger, and U. Schmidt, Preferred-frame and *CP*-violation tests with polarized electrons, Phys. Rev. D **78**, 092006 (2008).
[84] S. G. Turyshev and J. G. Williams, Space-based tests of gravity with laser ranging, Int. J. Mod. Phys. D **16**, 2165 (2007).
[85] T. B. Arp, C. A. Hagedorn, S. SCHLamminger, and J. H. Gundlach, A reference-beam autocollimator with nano-radian sensitivity from mHz to kHz and dynamic range of 10^7, Rev. Sci. Instrum. **84**, 095007 (2013).
[86] J. M. Hogan, J. Hammer, S.-W. Chiow, S. Dickerson, D. M. S. Johnson, T. Kovachy, A. Sugarbaker, and M. A. Kasevich, Precision angle sensor using an optical lever inside a Sagnac interferometer, Opt. Lett. **36**, 1698 (2011).
[87] J. Aasi *et al.* (LIGO Scientific Collaboration), Advanced LIGO, Classical Quantum Gravity **32**, 115012 (2015).
[88] M. Kasevich and S. Chu, Atomic Interferometry Using Stimulated Raman Transitions, Phys. Rev. Lett. **67**, 181 (1991).
[89] S. Dimopoulos, P. W. Graham, J. M. Hogan, and M. A. Kasevich, Testing General Relativity with Atom Interferometry, Phys. Rev. Lett. **98**, 111102 (2007).
[90] S. Dimopoulos, P. W. Graham, J. M. Hogan, M. A. Kasevich, and S. Rajendran, Gravitational wave detection with atom interferometry, Phys. Lett. B **678**, 37 (2009).
[91] S. Dimopoulos, P. W. Graham, J. M. Hogan, M. A. Kasevich, and S. Rajendran, An atomic gravitational wave interferometric sensor (AGIS), Phys. Rev. D **78**, 122002 (2008).
[92] S.-W. Chiow, T. Kovachy, H.-C. Chien, and M. A. Kasevich, $102\hbar k$ Large Area Atom Interferometers, Phys. Rev. Lett. **107**, 130403 (2011).
[93] S. M. Dickerson, J. M. Hogan, A. Sugarbaker, D. M. S. Johnson, and M. A. Kasevich, Multiaxis Inertial Sensing with Long-Time Point Source Atom Interferometry, Phys. Rev. Lett. **111**, 083001 (2013).
[94] S. Dimopoulos, P. W. Graham, J. M. Hogan, and M. A. Kasevich, General relativistic effects in atom interferometry, Phys. Rev. D **78**, 042003 (2008).
[95] A. Sugarbaker, S. M. Dickerson, J. M. Hogan, D. M. S. Johnson, and M. A. Kasevich, Enhanced Atom Interferometer Readout through the Application of Phase Shear, Phys. Rev. Lett. **111**, 113002 (2013).
[96] T. Kovachy, J. M. Hogan, A. Sugarbaker, S. M. Dickerson, C. A. Donnelly, C. Overstreet, and M. A. Kasevich, Matter Wave Lensing to Picokelvin Temperatures, Phys. Rev. Lett. **114**, 143004 (2015).
[97] P. W. Graham, J. M. Hogan, M. A. Kasevich, and S. Rajendran, A New Method for Gravitational Wave Detection with Atomic Sensors, Phys. Rev. Lett. **110**, 171102 (2013).
[98] J. G. Williams, S. G. Turyshev, and D. H. Boggs, Lunar laser ranging tests of the equivalence principle with the Earth and Moon, Int. J. Mod. Phys. D **18**, 1129 (2009).

[99] R. W. Hellings and G. S. Downs, Upper limits on the isotropic gravitational radiation background from pulsar timing analysis, Astrophys. J. **265**, L39 (1983).

[100] C. J. Moore, S. R. Taylor, and J. R. Gair, Estimating the sensitivity of pulsar timing arrays, Classical Quantum Gravity **32**, 055004 (2015).

[101] A. Khmelnitsky and V. Rubakov, Pulsar timing signal from ultralight scalar dark matter, J. Cosmol. Astropart. Phys. 02 (2014) 019.

[102] N. K. Porayko and K. A. Postnov, Constraints on ultralight scalar dark matter from pulsar timing, Phys. Rev. D **90**, 062008 (2014).

[103] C. L. Carilli and S. Rawlings, Science with the Square Kilometer Array: Motivation, key science projects, standards and assumptions, New Astron. Rev. **48**, 979 (2004).

[104] C. J. Moore, R. H. Cole, and C. P. L. Berry, Gravitational-wave sensitivity curves, Classical Quantum Gravity **32**, 015014 (2015).

[105] R. Penrose, Gravitational collapse: The role of general relativity, Riv. Nuovo Cimento **1**, 252 (1969) Gen. Relativ. Gravit. **34**, 1141 (2002).

[106] L. F. Abbott, A Mechanism for reducing the value of the cosmological constant, Phys. Lett. B **150**, 427 (1985).

[107] D. J. E. Marsh and J. Silk, A model for halo formation with axion mixed dark matter, Mon. Not. R. Astron. Soc. **437**, 2652 (2014).

[108] E. G. Adelberger, Torsion-Balance Probes of Fundamental Physics, in *Proceedings of Community Summer Study 2013: Snowmass on the Mississippi (CsS^{2}013) Minneapolis, MN, 2013* (to be published), arXiv:1308.3213.

[109] J. Chiaverini, S. J. Smullin, A. A. Geraci, D. M. Weld, and A. Kapitulnik, New Experimental Constraints on Non-Newtonian Forces below 100 microns, Phys. Rev. Lett. **90**, 151101 (2003).

[110] S. Thomas, in *Axions 2010: Proceedings of the International Conference*, edited by D. B. Tanner and K. A. van Bibber, AIP Conf. Proc. No. 1274 (AIP, New York, 2010).

[111] P. Sikivie, N. Sullivan, and D. Tanner, Proposal for Axion Dark Matter Detection Using an LC Circuit, Phys. Rev. Lett. **112**, 131301 (2014).